Q. J. R. Meteorol. Soc. (1995), 121, pp. 23–53 551.574.1:551.558:551.501.7

Diagnosis of hydrometeor profiles from area-mean vertical-velocity data

By SCOTT A. BRAUN* and ROBERT A. HOUZE Jr
University of Washington, USA

(Received 7 January 1994; revised 31 May 1994)

SUMMARY

A simple one-dimensional microphysical retrieval model is developed for estimating vertical profiles of liquid and frozen hydrometeor mixing ratios from observed vertical profiles of area-mean vertical velocity in regions of convective and/or stratiform precipitation. The mean vertical-velocity profiles can be obtained from Doppler radar (single and dual) or other means. The one-dimensional results are shown to be in good agreement with two-dimensional microphysical fields from a previous study. Sensitivity tests are performed.

1. INTRODUCTION

The diagnosis of bulk properties of convective systems has been a long-standing problem in the understanding of the interactions between organized cumulus convection and large-scale motions. In the tropics, organized convection is important for the development and maintenance of the larger-scale circulations, and the balance of the global heat budget (Riehl and Malkus 1958). Palmén and Newton (1969) and Houze (1973) suggested that convection also contributes significantly to the vertical transports of heat and momentum at midlatitudes. Fritsch *et al.* (1986) have shown that mesoscale convective systems (MCSs) account for up to 70% of the warm-season rainfall in the United States east of the Rockies. Therefore, knowledge of the bulk properties of these convective systems is important for the accurate parametrization of organized convection in larger-scale models.

With the advent of spaceborne passive microwave radiometers and radars on satellites, the measurement of rainfall from space should be improved significantly. The Tropical Rainfall Measuring Mission (TRMM) (Simpson *et al.* 1988) is a satellite program designed to obtain high-resolution measurements of tropical precipitation from space, and there is much ongoing work to provide ground truth for the TRMM satellite (Thiele 1987). An important part of the TRMM ground-truth research will be the determination of the influence of the vertical distribution of hydrometeors (both liquid water and ice) within convection on the upwelling radiation observed by satellite. Wilheit *et al.* (1982), Hakkarinen and Adler (1988), Fulton and Heymsfield (1991), and Smith *et al.* (1992) have shown that brightness temperatures measured by microwave radiometers are sensitive to the presence of both rain at low levels and precipitating ice aloft. However, direct observations of the vertical distribution of hydrometeors within convective systems are scarce (Heymsfield and Hjelmfelt 1984). Therefore, an indirect method to derive information on hydrometeors in convective clouds from other data is highly desirable.

Previous studies have described diagnostic methods for determining the bulk properties of convective and stratiform clouds associated with mesoscale convective systems. Cloud properties have been deduced from four basic sources in these studies: (1) large-scale heat budgets, (2) radar reflectivity measurements, (3) kinematic models, and (4) thermodynamic and microphysical retrievals. Each approach is described below.

* Corresponding author: Department of Atmospheric Sciences, AK-40, University of Washington, Seattle, WA 98195, USA.

Yanai *et al.* (1973) used a simple convective-cloud model to infer bulk properties of tropical cloud clusters from rawinsonde-based estimates of the large-scale heat source, Q_1, and moisture sink, Q_2. They calculated the mean cloud mass flux, moist static energy, cloud liquid water, and precipitation liquid water. Their model did not account for the presence of ice, and therefore could not address the vertical distribution of frozen hydrometeors. Furthermore, it did not include the effects of mesoscale precipitation areas, which frequently contain large areas of stratiform as well as convective precipitation. Therefore, the application of their model to observed Q_1 and Q_2 profiles, which do include the effects of the stratiform precipitation regions, led to errors in the computation of convective-cloud properties (Johnson 1984).

Austin and Houze (1973) introduced a method for determining the vertical mass flux and vertical transports of heat and momentum from radar and rain-gauge observations of precipitation in convective systems. The basic premise was that the amount of lifting within convective cells was related to the precipitation they produced. Cloud liquid water amounts were obtained from an equation for the conservation of water. However, this method did not distinguish liquid water from ice and yielded no information on the vertical distribution of the different hydrometeor types (e.g. rain versus snow).

Churchill and Houze (1984) deduced updraught magnitudes and cloud ice contents within an upper-tropospheric stratiform cloud deck in a tropical MCS from radar reflectivity at upper levels. Using a formulation of the ice budget of the stratiform region, they diagnosed mesoscale ascent of up to 23 cm s^{-1} and cloud ice contents of 0.1 to 0.3 g m^{-3}. However, their analysis was applied to a single level only and may not be applicable to convective precipitation regions.

Houze *et al.* (1980) and Leary and Houze (1980) extended the methods of Austin and Houze (1973) and Yanai *et al.* (1973) to account for the effects of both the convective and stratiform precipitation regions of MCSs. The model was based on the water budget of convective clouds with associated stratiform precipitation. This formulation could be used with either synoptic-scale measurements of the large-scale heating or measurements of precipitation from radar as input. Cloud liquid water and precipitation liquid water were estimated from diagnosed cloud-mean vertical motions and a simple warm-cloud bulk parametrization of the precipitation process. Again, ice was not included.

With the advent of Doppler weather radar, which provides information on both the precipitation and kinematic structures of convective systems, additional information became available for diagnosing the thermodynamic and microphysical properties of convective systems. In the past few years, kinematic models (Rutledge and Hobbs 1983, 1984; Ziegler 1985; Rutledge and Houze 1987) and thermodynamic and microphysical retrieval methods (Gal-Chen 1982; Roux *et al.* 1984; Hauser *et al.* 1988; Braun and Houze 1994, hereafter referred to as BH94) have been applied to detailed dual-Doppler synthesized velocity fields and have yielded significant new insights into the thermodynamic and microphysical properties of convective systems. Hauser *et al.* (1988) developed a method for simultaneously retrieving the thermodynamic and microphysical properties of a convective storm using dual-Doppler synthesized velocities as input. Chong and Hauser (1989, 1990) then used the retrieved microphysical variables to deduce the water and heat budgets of the squall line. Disadvantages of their analyses were that the effects of ice within the convective region were not considered and that the convective and stratiform precipitation regions were analysed separately.

BH94 recently used these retrieval methods to diagnose the precipitation structure of a midlatitude squall line with trailing stratiform precipitation which occurred on 10–11 June 1985 during the PRE-STORM (Preliminary Regional Experiment for the STormscale Operational and Research Meteorology (Cunning (1986)). The microphysical

retrieval method, applied in two dimensions (x-z) and under assumed steady-state conditions, allowed for the diagnosis of liquid (cloud and rain water) and frozen (cloud and precipitating ice) hydrometeor species simultaneously in both the convective and stratiform precipitation regions. Potential temperature and pressure were also retrieved. Radar reflectivities computed from the retrieved precipitation mixing ratios compared well with the observed radar reflectivity (BH94). While the microphysical retrieval method was useful for diagnosing the mean structure of a convective system with relatively simple organization of precipitation (leading line/trailing stratiform precipitation), it may be difficult to apply to systems with more complicated organization since microphysical calculations of the type performed by BH94 over large areas in three dimensions are difficult. It is also difficult to obtain meaningful retrievals in the rapidly changing convective areas of the storm because of limitations on the scanning rates of present-day radars (Sun and Houze 1992), i.e. the time interval required for meaningful estimates of the time derivatives is generally much smaller than the time required to scan the vertical structure of a storm.

Situations arise in which the mean properties of a convective system are sufficient for analysis, e.g. when estimating area-mean heating rates (Tao *et al.* 1990, 1993; Braun and Houze 1995) and when applying radiative-transfer models to data from spaceborne microwave sensors (Olsen 1989) to retrieve rainfall rates. In such situations one-dimensional (1-D) models can be utilized to diagnose vertical profiles of the mean microphysical variables, even if the three-dimensional (3-D) details of the storm structure are difficult to determine. Zrnic *et al.* (1993) used a 1-D kinematic model to diagnose the mean microphysical structure of the stratiform precipitation region of a PRE-STORM squall line in Oklahoma on 3 June 1985; however, their method may not be applicable to regions of convection. In this study we propose a method for diagnosing vertical profiles of area-averaged hydrometeor mixing ratios in *both* convective and stratiform precipitation regions of MCSs from vertical profiles of area-mean vertical velocity. These mean vertical-velocity profiles can be obtained directly from Doppler radar data or from vertical mass fluxes estimated following the methods outlined in Austin and Houze (1973) or Houze *et al.* (1980). Since the method uses only the area-averaged vertical velocity as input, detailed multiple-Doppler synthesis of the wind fields is not required. A vertical profile of divergence obtained by a single Doppler radar and integrated to give an area-wide mean vertical air motion would be sufficient. Note: methods such as VAD and EVAD (Velocity Azimuth Display and Extended Velocity Azimuth Display, Srivastava *et al.* 1986), which cannot be applied to regions of convection, are not required to obtain area-mean divergence from a single Doppler radar (see section 5(c)).

While information is lost in going from three dimensions to one dimension, the proposed 1-D retrieval method has advantages in that the method can be applied to convective systems with any mode of organization, that the computations can be done very quickly compared with retrievals from 2-D and 3-D wind fields, and that the input data requirements are much less stringent. The 1-D retrieval results, moreover, can be readily combined with a radiative-transfer model to improve retrieval of rainfall rates from brightness temperatures measured by microwave sensors. Also, the microphysical parametrizations allow for the determination of the vertical distribution of heating rates. For example, the melting and freezing rates for a midlatitude squall line are examined by Braun and Houze (1995). In section 2 the 1-D retrieval model is described and the governing equations are derived. In section 3 we verify the results of the 1-D model by comparing the results with the 2-D retrieval results of BH94. In section 4 some sensitivity tests are performed, and in section 5 the possible applications of the 1-D retrieval model are discussed. Finally, conclusions are given in section 6.

2. Conceptual framework and retrieval equations

The 1-D retrieval model is formulated generally following Ferrier and Houze (1989). However, the model is expressed in Cartesian (x, y, z) rather than polar coordinates. The Cartesian coordinate system is chosen in order to be able to apply the model to a large arbitrarily shaped region rather than only to an individual convective cell. The retrieval model is used to diagnose mixing ratios (in kg water/kg air) of total water (q_T), rain (q_r), precipitating ice (q_p), and cloud ice (q_i), from which cloud water (q_c) and water vapour (q_v) are then determined.

If χ_c represents the value of any of the microphysical fields, the horizontally averaged value of χ_c over a region of area A is

$$\bar{\chi}_c = \frac{1}{A}\int_A \chi_c \, d\sigma \tag{1}$$

where $d\sigma$ is an element of area. The average of χ_c along the outer boundary of A with perimeter length L is

$$\overline{\bar{\chi}}_c = \frac{1}{L}\oint_L \chi_c \, dl \tag{2}$$

where dl is an element of length. Deviations of χ_c from $\bar{\chi}_c$ and $\overline{\bar{\chi}}_c$ are denoted by χ_c' and χ_c'', respectively.

The 3-D anelastic continuity equation in Cartesian coordinates is

$$\nabla_h \cdot \mathbf{V} + \frac{1}{\rho_e}\frac{\partial(\rho_e w)}{\partial z} = 0 \tag{3}$$

where $\mathbf{V} = (u, v)$, $\nabla_h = (\partial/\partial x, \partial/\partial y)$, x and y are the horizontal coordinates, u and v are the x and y components of velocity, z is the vertical coordinate, w is the vertical velocity, and ρ_e is the density of the environment, assumed to be a function of height only. Applying (1) and (2) to (3) gives the area-averaged form of the continuity equation

$$\frac{L}{A}\overline{\bar{V}}_n + \frac{1}{\rho_e}\frac{\partial(\rho_e \bar{w})}{\partial z} = 0 \tag{4}$$

where the subscript 'n' indicates the component of the velocity normal to the boundary, defined to be positive when directed out of the area.

The material derivative of the in-cloud quantity χ_c expressed in Cartesian coordinates can be combined with (3) to obtain

$$\frac{D\chi_c}{Dt} = \frac{\partial\chi_c}{\partial t} + \nabla_h \cdot (\mathbf{V}\chi_c) + \frac{1}{\rho_e}\frac{\partial(\rho_e w \chi_c)}{\partial z}. \tag{5}$$

Applying (1) to (5) and making use of (2) yields

$$\overline{\frac{D\chi_c}{Dt}} = \frac{\partial\bar{\chi}_c}{\partial t} + \frac{L}{A}\overline{\bar{V}_n\chi_c} + \frac{1}{\rho_e}\frac{\partial(\rho_e\overline{w\chi_c})}{\partial z}. \tag{6}$$

The second and third terms on the right-hand side of (6) can be expressed in terms of their mean and eddy components

$$\frac{L}{A}\overline{\bar{V}_n\chi_c} = \frac{L}{A}\overline{\bar{V}}_n\bar{\chi}_c + \frac{L}{A}\overline{\bar{V}_n''\chi_c''} \tag{7}$$

$$\frac{1}{\rho_e}\frac{\partial(\rho_e\overline{w\chi_c})}{\partial z} = \frac{1}{\rho_e}\frac{\partial(\rho_e\bar{w}\bar{\chi}_c)}{\partial z} + \frac{1}{\rho_e}\frac{\partial(\rho_e\overline{w'\chi_c'})}{\partial z}. \tag{8}$$

The vertical eddy flux term can be parametrized by

$$\frac{1}{\rho_e}\frac{\partial(\rho_e\overline{w'\chi_c'})}{\partial z} = -\frac{\partial}{\partial z}\left(K\frac{\partial\bar{\chi}_c}{\partial z}\right) \tag{9}$$

where K is the eddy mixing coefficient. Substitution from (4) expresses the first term on the right-hand side of (7) in terms of $\bar{w}$ and $\bar{\bar{\chi}}_c$. The second term on the right-hand side of (7) is then the only term that is difficult to express in terms of $\bar{w}$, $\bar{\chi}_c$, or $\bar{\bar{\chi}}_c$. Under certain circumstances the term $\overline{\overline{V_n''\chi_c''}}$ is negligible. For example, if the boundary of the averaging domain is in clear air surrounding a region of convection, then this term is exactly zero (as is $\bar{\bar{V}}_n\bar{\chi}_c$) when χ_c represents the mixing ratio of a hydrometeor species. If the boundary resides in relatively uniform stratiform precipitation surrounding convection, then the horizontal eddy flux term becomes negligible. However, since significant variations of χ_c can exist along the boundary in other regions of precipitation (e.g. if the boundary lies in a region of convection), we cannot assume *a priori* that the horizontal eddy flux term is negligible.

In Eq. (6) the horizontal flux term is proportional to the ratio of the perimeter length to the area of the averaging domain. This term is thus similar to entrainment in plume models of convection, in which entrainment is proportional to the surface-to-volume ratio. Therefore, we anticipate that as the averaging area is increased, the importance of the horizontal flux terms diminishes.

For the case in which χ_c represents a precipitation mixing ratio, the relative magnitudes of the horizontal and vertical flux terms in (6) can be compared by using dual-Doppler synthesized velocity and radar-reflectivity data for the convective and stratiform regions of a squall line. To make such a comparison we use dual-Doppler data from the 10–11 June 1985 squall line (Rutledge *et al.* 1988a; Johnson and Hamilton 1988; Biggerstaff and Houze 1991a, 1991b, 1993; BH94). Figures 1(a) and 2(a) show the radar reflectivity at 1.4 km above mean sea level in the convective region at 0131 UTC and in the stratiform region at 0345 UTC 11 June, respectively. To simplify the calculations the averaging areas are taken to be rectangular, as indicated in the figures. Precipitation mixing ratios are estimated from the radar-reflectivity factor using Rogers and Yau's (1989, p. 191) relationship for rain,

$$q_r = \frac{3.92\times10^{-6}}{\rho_e}Z^{0.55} \tag{10}$$

where Z is in $\mathrm{mm^6m^{-3}}$ and q_r is in $\mathrm{kg\,kg^{-1}}$. Environmental quantities (e.g. ρ_e) are taken from a sounding at Enid, Oklahoma, at 0134 UTC 11 June 1985 (Fig. 3). This sounding, taken ahead of the storm, is discussed in more detail by Sun *et al.* (1993). In the stratiform region, mixing ratios within the melting layer are interpolated from estimated values immediately above and below the radar bright band. Equation (10) is applied at all levels; however, computations including a q–Z relationship for ice produced similar results. Below 5.4 km, missing velocity data along the boundaries in precipitation-free regions ahead of the convective line are replaced by the velocities measured by the Enid sounding. Calculations of the total vertical flux (left-hand side of (8)) are made only at heights where no more than 20% of the velocity and reflectivity data are missing within the averaging area. The horizontal flux terms (all terms in (7)) are computed at heights where no more than 20% of the velocity and reflectivity data are missing along any

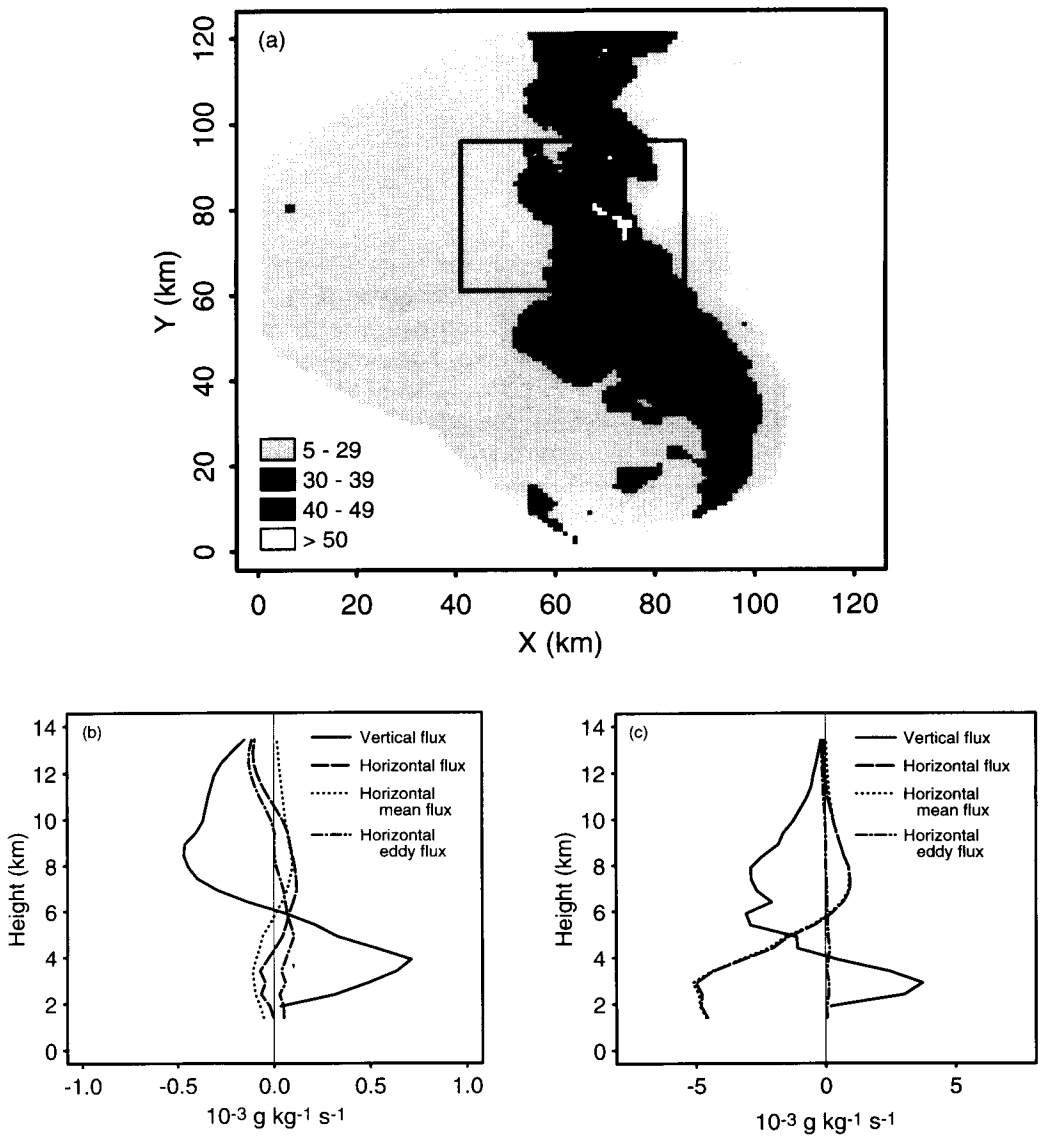

Figure 1. (a) Convective region radar reflectivity (dBZ) at 1.4 km above mean sea level for the dual-Doppler analysis at 0131 UTC 11 June 1985. The box indicates the averaging area used to compute the profiles in (b) and (c). (b) Vertical profiles of the vertical and horizontal flux of precipitation for 0131 UTC. The mean and eddy components of the horizontal flux are also shown. (c) Same as in (b), but for the total water mixing ratio.

segment of the rectangular boundary, except below 5.4 km ahead of the convective line where velocity data from the Enid sounding are used.

Figure 1(b) shows profiles of the total vertical and total horizontal fluxes (left-hand sides of (7) and (8)) determined from the dual-Doppler volume at 0131 UTC within the area indicated by the rectangle in Fig. 1(a). The mean and eddy components of the horizontal flux (right-hand side of (7)) are also indicated. The profiles show that within the convective region the horizontal flux tends to be much smaller than the vertical flux. In the stratiform region (Fig. 2(b)), the total horizontal and vertical fluxes are nearly equal but opposite in sign, and the total horizontal flux tends to be dominated by the

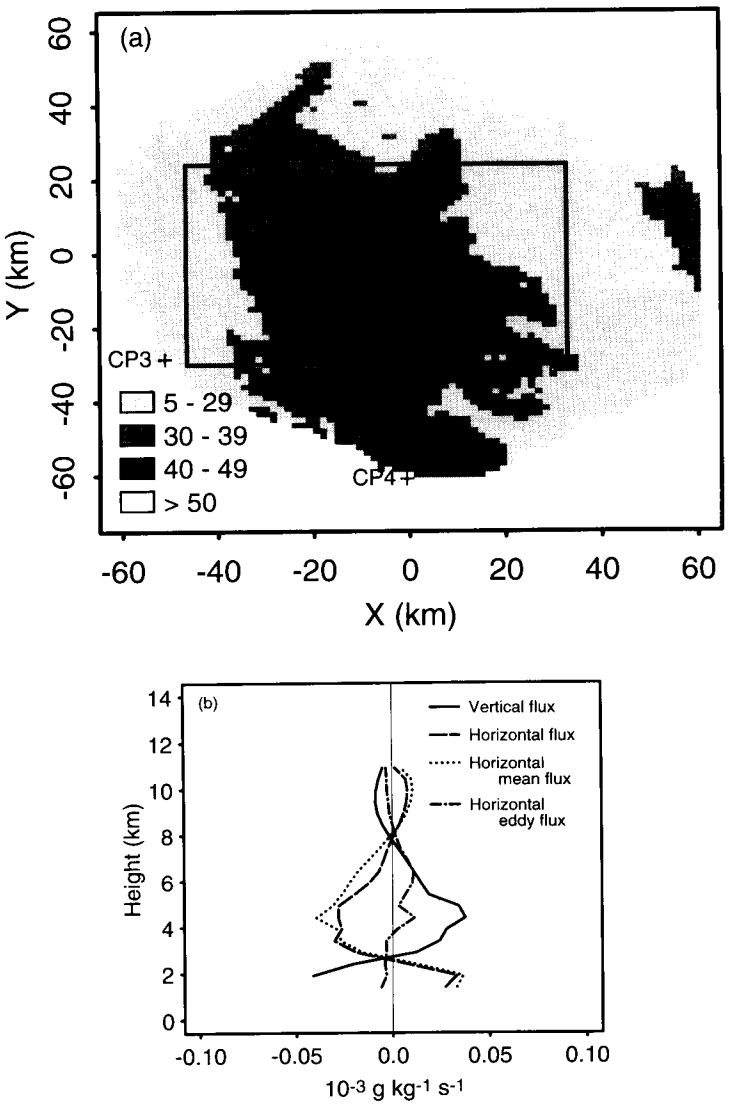

Figure 2. Same as in Figs. 1(a) and (b), but for the stratiform precipitation region at 0345 UTC 11 June 1985. The locations of the CP-3 and CP-4 radars at this time are indicated by the '+' symbols.

mean component. These results suggest that, to a first approximation, Eq. (6) can be solved for the precipitation mixing ratios by neglecting the eddy component of the horizontal flux, which cannot be readily computed or parametrized. We assume that the horizontal eddy flux term is also small for cloud ice. A similar assumption was made by Churchill and Houze (1984) in their diagnostic study of the stratiform region of a tropical MCS. Sensitivity tests described in section 4 support this assumption.

For the total-water mixing ratio, the horizontal flux cannot be ignored, largely because of the contribution from water vapour. To demonstrate the importance of the horizontal flux in the equation for the total-water mixing ratio, we approximated the total water field from the Doppler radar data at 0131 UTC (Fig. 1(a)) by adding the saturation vapour mixing ratio from the Enid sounding to the precipitation mixing ratios

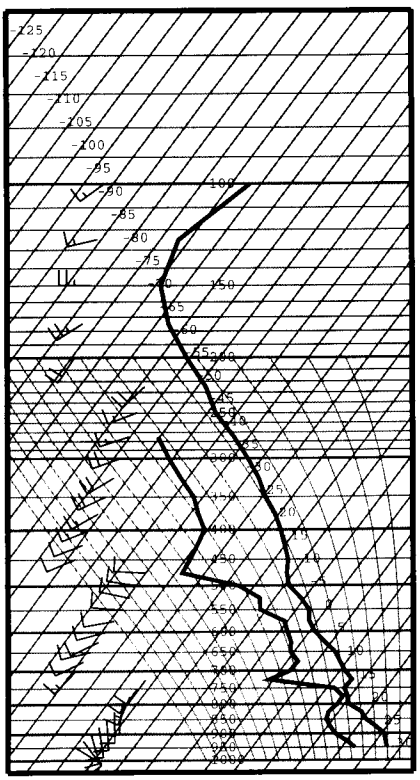

Figure 3. Skew T–log p profiles of temperature, dew-point temperature, and winds for Enid, Oklahoma at 0134 UTC 11 June 1985. For wind speed, one full barb = 5 m s^{-1} and one half barb = 2.5 m s^{-1}.

estimated from (10). Figure 1(c), which shows the profiles of the horizontal and vertical fluxes of total-water mixing ratio, indicates that the horizontal flux of total water is quite important, especially at low levels where the vapour mixing ratio is large. The horizontal eddy flux is small since we did not account for variations of the vapour mixing ratio along the boundary. However, we anticipate that this term would also be small when variations of water vapour are taken into account.

If we assume that the eddy component of the horizontal flux in (7) is negligible and that the eddy component of the vertical flux is parametrizable according to (9), then substituting (4), (7), (8), and (9) into (6) yields

$$\frac{\overline{\mathrm{D}\chi_c}}{\mathrm{D}t} = \frac{\partial \bar{\chi}_c}{\partial t} + \bar{w}\frac{\partial \bar{\chi}_c}{\partial z} + \frac{1}{\rho_e}\frac{\partial(\rho_e \overline{w})}{\partial z}(\bar{\chi}_c - \overline{\bar{\chi}_c}) - \frac{\partial}{\partial z}\left(K\frac{\partial \bar{\chi}_c}{\partial z}\right). \tag{11}$$

The term $\overline{\bar{\chi}_c}$ is approximated by setting its value proportional to the in-cloud value, $\bar{\chi}_c$,

$$\overline{\bar{\chi}_c} = \alpha \bar{\chi}_c \tag{12}$$

where α is a proportionality constant. $\alpha = 0$ corresponds to a situation in which the boundary resides in clear air surrounding the cloud and precipitation, while $\alpha = 1$ corresponds to a top-hat distribution across a convective region or to a boundary entirely within a region of uniform stratiform precipitation. For the case examined in this study (i.e. the 10–11 June 1985 squall line), estimates of the precipitation mixing ratios from radar reflectivity and from the retrieval analysis of BH94 suggest a value of $\alpha \approx 0.5$ for

rain and precipitating ice in the convective region. The retrieval results of BH94 further suggest that in the convective region α is approximately unity for cloud ice, while for the total-water mixing ratio α tends to be near unity below the melting level and about 0.8 above that level. In the stratiform region, $\alpha = 1$. In section 4 we will show that results for the convective region are generally not sensitive to the values of α used for rain, precipitating ice, and cloud ice.

To solve (11) we assume stationarity of the area-mean conditions, i.e. that the time rates of change of the area-mean mixing-ratio fields are small compared with the other terms on the right-hand side of (11). This assumption should be most nearly valid when the convection is at, or near, maturity. Furthermore, since stationarity requires only that the area-mean mixing ratios are steady, this assumption is less restrictive than steady-state assumptions for calculations in two or three dimensions, which require constant values at every grid point. The stationarity assumption yields the following equations for the 1-D microphysical retrieval. For rain, precipitation ice, and cloud ice, we have

$$\overline{w}\frac{\partial \overline{q}}{\partial z} - \frac{\partial}{\partial z}\left(K\frac{\partial \overline{q}}{\partial z}\right) + \frac{1}{\rho_e}\frac{\partial(\rho_e \overline{w})}{\partial z}(\overline{q} - \alpha\overline{q}) = \overline{S}_q + \frac{1}{\rho_e}\frac{\partial}{\partial z}(\rho_e \overline{V}_q \overline{q}) \tag{13}$$

where $q = (q_r, q_p, q_i)$, V_q is the terminal fall speed of rain (V_r) or precipitating ice (V_p), and S_q is the source term for rain, precipitating ice, or cloud ice. Note that the stratiform-region profiles of the vertical and horizontal fluxes in Fig. 2(b) indicate that the dominant balance in (13) in the stratiform region is between the rate at which precipitation is produced and the rate at which it is lost because of fallout (i.e. the sum of the terms on the left-hand side of (13) is near zero). The equation for the total-water mixing ratio is

$$\begin{aligned}\overline{w}\frac{\partial \overline{q}_T}{\partial z} - \frac{\partial}{\partial z}\left(K\frac{\partial \overline{q}_T}{\partial z}\right) + \frac{1}{\rho_e}\frac{\partial(\rho_e \overline{w})}{\partial z}(\overline{q}_T - \alpha\overline{q}_T) = \\ + \frac{1}{\rho_e}\frac{\partial}{\partial z}(\rho_e \overline{V}_r \overline{q}_r) + \frac{1}{\rho_e}\frac{\partial}{\partial z}(\rho_e \overline{V}_p \overline{q}_p).\end{aligned} \tag{14}$$

Mixing ratios for q_v and q_c are not determined explicitly. Instead, using the definition of q_T, they are computed from (Hauser *et al.* 1988; Marécal *et al.* 1993; BH94)

$$q' = q_T - q_r - q_p - q_i - q_{vs} \tag{15}$$

where q_{vs} is the saturation water vapour mixing ratio and is determined following the formulation of Tetens (1930). If $q' > 0$, then $q_c = q'$, $q_v = q_{vs}$. If $q' < 0$, then $q_c = 0$, and $q_v = q' - q_r - q_p - q_i$.

The microphysical source terms are parametrized using the bulk microphysical parametrizations of Lin *et al.* (1983) for rain and precipitating ice (applying the fall-speed relationship for an arbitrary form of precipitating ice to their parametrizations for snow), with the following exceptions. Autoconversion of cloud water to rain is parametrized following Kessler (1969). Evaporation of melting precipitating ice is included following Rutledge and Hobbs (1983). The initiation and depositional growth of cloud ice is parametrized following Rutledge and Hobbs (1983).

In (13) we implicitly assume that the microphysical source terms can be estimated from the area-mean mixing ratios and thermodynamic variables, i.e. that

$$\overline{S_q(q_r, q_p, \ldots, T, p)} = S_q(\overline{q}_r, \overline{q}_p, \ldots, \overline{T}, \overline{p}). \tag{16}$$

In other words, the area-mean source terms determined by computing the source terms at each point in x and y and then averaging over area is approximated by computing the source terms from the area-mean mixing ratios, temperature, and pressure. To test this

assumption and determine its limitations, we use two sets of information from the microphysical retrievals discussed in BH94. The first set of information consists of the microphysical retrieval results of BH94 for the 10–11 June 1985 squall line (the rain and precipitating-ice fields are shown in Fig. 4(a)). The second set of information consists of the microphysical fields retrieved from the wind and thermodynamic fields of the model simulation of Fovell and Ogura (1988) and presented as verification of the 2-D retrieval in BH94 (Fig. 4(b)). The reason for the two sets of information will be apparent in the discussion below. The procedure that we use is to calculate the microphysical source terms at each point in the convective region, taken as the region between $x = 40$ and 105 km in Fig. 4(a) and $x = -32$ to -6 km in Fig. 4(b), and then average these terms to obtain profiles of the mean source terms (left-hand side of (16), hereafter referred to as $\overline{S}_q$). Next, we average the mixing ratio and thermodynamic fields and then compute the microphysical source terms (right-hand side of (16), hereafter referred to as $S_{\overline{q}}$).

In short, very good agreement was found between profiles of $S_{\overline{q}}$ and $\overline{S}_q$ for each microphysical term (e.g. rain evaporation and collection of cloud water by rain) except for the terms for autoconversion of cloud water to rain, melting of precipitating ice, and accretion of rain by precipitating ice. For the autoconversion term, the autoconversion rate was zero when computed from the area-averaged cloud water mixing ratios since this mixing ratio did not exceed the threshold value (taken as 0.5 g kg^{-1} by BH94). On the other hand, in the 2-D cloud-water field of BH94 (see their Fig. 6(d)), regions of cloud-water mixing ratios greater than 0.5 g kg^{-1} were present at individual grid points, such that the mean autoconversion rate was nonzero. Agreement between the autoconversion rates was obtained by decreasing the threshold cloud-water mixing ratio from 0.5 to 0.2 g kg^{-1} for the 1-D calculations.

To discuss the melting and accretion terms, we show the total source term for precipitating ice (Fig. 5). The profiles of $S_{\overline{q}}$ and $\overline{S}_q$ show very good agreement for the 10–11 June data (Fig. 5(a)); however, for the Fovell and Ogura model output (Fig. 5(b)), substantial overestimates of the melting (strong negative values) and accretion of rain by precipitating ice (strong positive values) are apparent. The errors in the latter case were found to result from substantial horizontal variability of the temperature (>2 K) near the level of peak mean melting (2.5 km in Fig. 5(b)); only weak temperature variability was present in the 10–11 June data. To demonstrate this conclusion we removed the temperature variability in the Fovell and Ogura model results by computing $S_q(q_r, q_p, \ldots, \overline{\overline{T}}, \overline{p})$, i.e. the area-mean temperature and pressure were substituted for the temperature at each point. Figure 5(c) shows that the error in the melting term is nearly eliminated and the error in the accretion term is reduced when the temperature variability is removed. The errors (in Fig. 5(b)) are generally not caused by the variability of the precipitating-ice mixing ratios, which varied substantially near the melting level for both sets of retrieved microphysical fields. Further examination of the melting term also suggests that the sensitivity of the mean melting term to temperature variability decreases with decreasing mean precipitating-ice mixing ratio in the melting layer. For example, mean melting rates in the stratiform region were not sensitive to temperature variability because of smaller mean ice mixing ratios. This result implies that (16) will be most accurate when the temperature variability and the mean precipitating-ice mixing ratios in the melting layer are small.

The errors from (16) are expected to be substantially reduced in the 1-D retrieval since the relaxation method (described below) used to obtain the mixing-ratio profiles inherently produces vertical smoothing. To indicate how vertical smoothing might affect the retrieved mixing-ratio profiles and heating rates, Fig. 5(d) shows the vertical profiles from Fig. 5(b) after vertical smoothing has been applied. Since the melting and accretion

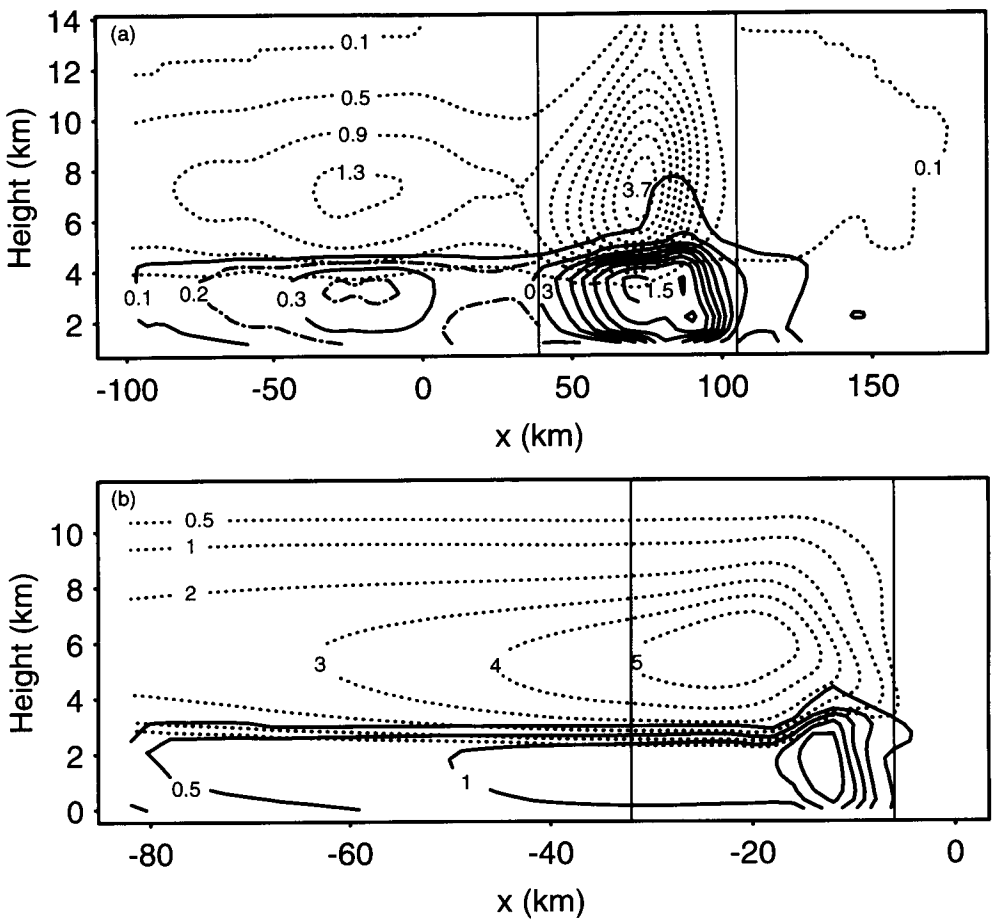

Figure 4. Retrieved mixing ratios of rain (solid) and precipitating ice (dotted) for (a) the 10–11 June 1985 squall line and (b) the cloud-model simulation of Fovell and Ogura (1988). In (a) contours are drawn every 0.2 g kg^{-1} for rain and every 0.4 g kg^{-1} for precipitating ice, starting at 0.1 g kg^{-1}. For rain, additional contours (dot-dashed) are drawn in the stratiform region at 0.2 and 0.4 g kg^{-1}. In (b) contours for snow are drawn at 1 g kg^{-1} intervals, with an additional contour at 0.5 g kg^{-1}. Contours for rain are at 0.5 g kg^{-1} intervals, with an additional contour at 0.1 g kg^{-1}. Vertical lines outline the convective regions.

terms are opposite in sign and nearly at adjacent grid points, the vertical smoothing produces significant cancellation of the errors in these terms.

Equations (13) and (14) are solved using centred finite differences and relaxation methods. The 1-D retrieval is run with a grid increment of 500 m, which is the vertical grid spacing of the dual-Doppler radar data used in this study. Since temperature and pressure are not being retrieved, these fields must be provided as input for the microphysical retrieval because they are necessary to estimate the microphysical source terms. With these inputs and a vertical profile of area-mean vertical velocity, the area-mean profiles of the hydrometeor mixing ratios can then be estimated by the 1-D retrieval model. As discussed by BH94, this type of diagnostic method simply seeks the microphysical fields that are instantaneously consistent with the radar-observed mean velocities and governing equations (13 and 14). The manner by which these fields evolve does not effect the calculations, in contrast to kinematic-model approaches, such as that used by Zrnic *et al.* (1993), which integrate the microphysical equations in time.

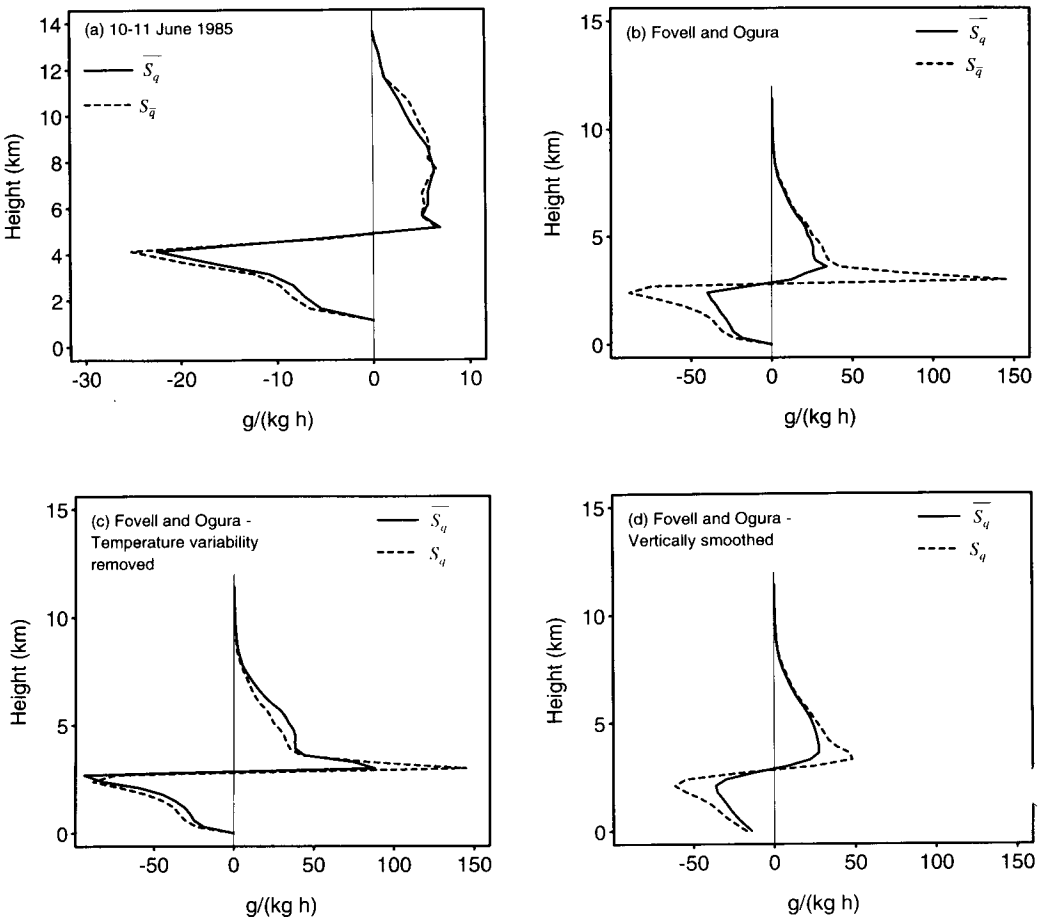

Figure 5. Profiles of the total production term for precipitating ice determined from microphysical retrievals for (a) the 10–11 June 1985 squall line (see Fig. 4(a)), (b) the Fovell and Ogura (1988) simulated squall line (see Fig. 4(b)), (c) the Fovell and Ogura simulated squall line with the temperature variation removed, and (d) the Fovell and Ogura simulated squall line with vertical smoothing. The $\overline{S_q}$ profile indicates the source term determined by calculating the source term at each point and then averaging over area (left-hand side of (16)) while the $S_{\bar{q}}$ profile indicates the source term calculated from the area-mean temperature and mixing-ratio profiles (right-hand side of (16)).

3. Verification

In this section we verify that the 1-D retrieval results are consistent with the 2-D results presented in BH94. Figure 6 shows a cross-section, oriented normal to the convective line, of the observed radar reflectivity and storm-relative airflow during the mature stage of the 10–11 June 1985 squall line. This cross-section is taken from a composite of the dual-Doppler reflectivity and velocity data (see Biggerstaff and Houze (1993) and BH94 for details). It corresponds to the cross-section of rain and precipitating ice in Fig. 4(a). Cross-sections of the retrieved potential temperature and pressure perturbations (from the pre-storm environment) and mixing ratios of water vapour, cloud water, and cloud ice are shown in Fig. 6 of BH94. A vertical-velocity profile (Fig. 7) is obtained by averaging the vertical velocity from the cross-section in Fig. 6 over $x = 40$ to 105 km (see vertical lines in Fig. 4(a)). This vertical-velocity profile shows maximum

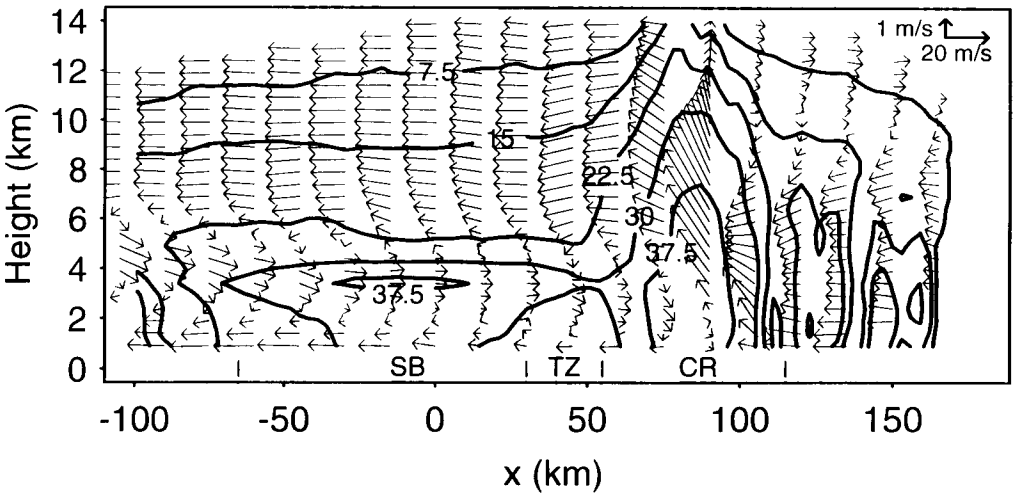

Figure 6. Along-line averaged radar reflectivity (dBZ) and storm-relative wind vectors in the plane of the cross-section. The arrows in the upper right corner represent the arrow scales corresponding to 1 m s $^{-1}$ for the vertical velocity and 20 m s $^{-1}$ for the horizontal velocity. The approximate positions of the secondary band (SB), transition zone (TZ), and convective region (CR) are indicated along the bottom of the figure.

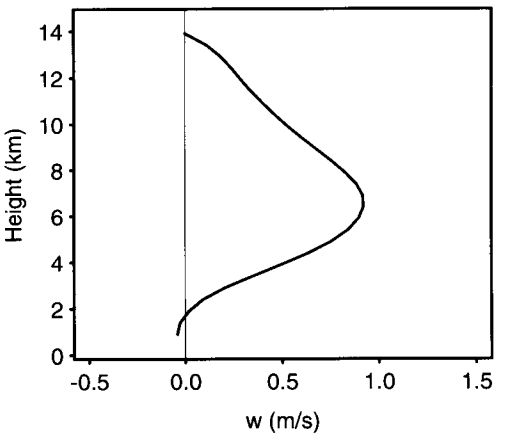

Figure 7. Mean convective region vertical velocity (m s^{-1}) determined by averaging the vertical velocities in Fig. 6 from $x = 40$ to 105 km.

mean ascent of approximately 0.9 m s^{-1} at an altitude of 6.6 km. We average the temperature and pressure from the 2-D retrieval over the same region to represent the convective-region temperature and pressure (Fig. 8). Mixing-ratio profiles for rain, precipitating ice, cloud water, and cloud ice averaged over the same domain from the 2-D retrieval (hereafter referred to as the 2-D results) are indicated by the thin lines in Fig. 9. These profiles provide the basis for comparison with the 1-D retrieval results.

The solution of (13) and (14) requires the specification of boundary conditions at the top and bottom of the column. At the top the mixing ratios of rain and cloud ice are set to zero, while the total-water mixing ratio is set equal to the sum of the average vapour and precipitating-ice mixing ratios from the 2-D results. In BH94 the upper boundary condition for precipitating ice was specified from the observed reflectivity field.

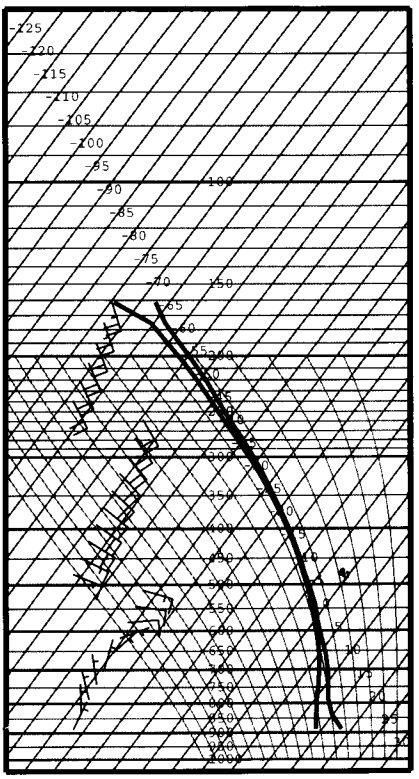

Figure 8. Skew T–log p profiles of the convective-region mean temperature, dew-point temperature, and winds averaged over $x = 40$ to 105 km (see Fig. 6) from the two-dimensional thermodynamic retrieval results of Braun and Houze (1994). Winds are storm-relative, with one full barb = 5 m s^{-1} and one half barb = 2.5 m s^{-1}.

For the purpose of verification the mixing ratio of precipitating ice at the top boundary is set equal to the average value from the 2-D results. In the sensitivity tests described below this value will be set to zero. At the bottom of the column (1.1 km), cloud ice and precipitating ice are set to zero. For rain and total water, constant vertical gradients are imposed at the lower boundary (similar to Marécal *et al.* 1993). Initial values for rain, precipitating ice, cloud water, and cloud ice are set to zero at interior points, while total water is set equal to the average vapour mixing ratio from the 2-D retrieval. Sensitivity tests indicate that the hydrometeor profiles are negligibly sensitive to the initial guesses for rain, precipitating ice, cloud water, and cloud ice; however, the results are sensitive to the initial guess for total water. The sensitivity to the initial total-water profile is discussed in detail in section 4. The mixing coefficient K is set to 2500 m^{2}s^{-1} as in BH94. The lump graupel fall-speed relationship of Heymsfield and Kajikawa (1987) is used for precipitating ice.* Since this relationship applies to the dimension of the particle, and particles are assumed to be exponentially distributed with respect to their melted diameter (Gunn and Marshall 1958), the Heymsfield and Kajikawa (1987) fall speed–diameter and mass–diameter relationships are combined following Potter (1991) so that the fall-speed relationship applies to the melted diameter rather than the particle dimension.

* Although this relationship was obtained for particles associated with frontal precipitation, the fall speeds compare well with those associated with graupel in convective storms (Heymsfield 1978).

The results of the 1-D retrieval, when applied to the average vertical-velocity profile in Fig. 7, are shown in Fig. 9 (thick lines), overlaid on the average mixing-ratio profiles from the 2-D retrieval results (thin lines). The mixing-ratio profiles from the 1-D model are generally similar to the 2-D results. The rain mixing ratios are underestimated by approximately 0.1 g kg^{-1}, except at the lowest grid point where the lower boundary value of q_r was held fixed in BH94. The precipitating-ice mixing ratios from the 1-D model reach a maximum value nearly identical to that in the 2-D results, but are underestimated above 7 km by about 0.2 to 0.3 g kg^{-1}. The cloud water amounts at mid-to-upper levels are slightly greater than the 2-D results and the 1-D model produces no cloud water below 3.6 km. The cloud-ice mixing ratios are somewhat greater than the average values from the 2-D results. In general, however, the agreement between the 1-D retrieval results and the average of the 2-D retrieval results is good.

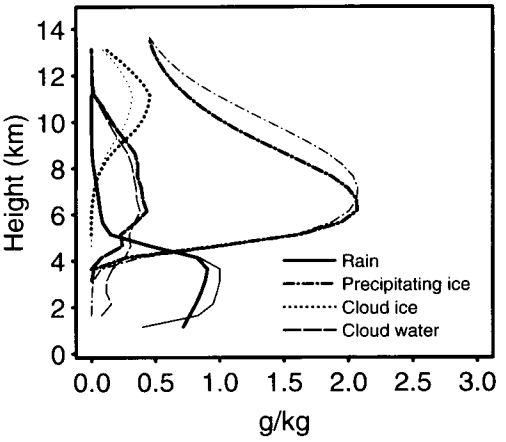

Figure 9. Hydrometeor mixing ratios (g kg^{-1}) determined from the one-dimensional retrieval model using the vertical-velocity profile in Fig. 7 as input. The average profiles from the two-dimensional retrieval are indicated by the thin lines.

4. Sensitivity tests

Tests are performed to determine the sensitivity of the 1-D retrieval results to six parameters: the mixing coefficient, the fall-speed relationship for precipitating ice, the input-temperature profile, the initial profile of total-water mixing ratio, the input vertical-velocity profile, and the values of α for rain, precipitating ice, and cloud ice. Profiles for a control case are obtained by using inputs identical to those in the verification described in the previous section, except that the upper boundary condition for precipitating ice is set to zero. Sixteen tests were conducted and are listed in Tables 1–3. The vertically integrated water contents (IWCs) of rain, precipitating ice, cloud water, and cloud ice are provided in the tables. The percentage changes, defined as $(IWC_j\text{-}IWC_0)/IWC_0$, where IWC_0 and IWC_j are the IWCs from the control case (unless indicated otherwise) and sensitivity test j, are also included in the tables. Unless stated otherwise the retrieved mixing-ratio profiles for each test are indicated in the following figures by thick lines, while the profiles for the control case are indicated by thin lines.

The first two cases test the sensitivity of the model results to the value of the mixing coefficient K which is important for the use of the relaxation methods in the solution of (13) and (14). A value of 2500 m^2s^{-1} was used in the control run. For case (i) (Fig. 10(a))

TABLE 1. SUMMARY OF SENSITIVITY TESTS (*i*)–(*v*)

Case	Description	IWC for q_r	IWC for q_p	IWC for q_c	IWC for q_i
	Control	2.64	5.45	1.19	0.68
(*i*)	Eddy mixing coefficient $K = 1500\ m^2 s^{-1}$	2.67	4.83	0.98	0.75
		1%	−11%	−18%	10%
(*ii*)	Eddy mixing coefficient $K = 3500\ m^2 s^{-1}$	2.67	5.59	1.19	0.68
		1%	3%	0%	0%
(*iii*)	Graupel-like snow fall-speed parameters ($a = 12.4$, $b = 0.42$)	2.19	11.17	1.43	0.53
		−17%	105%	20%	−22%
(*iv*)	Plates with dendritic extensions fall speed ($a = 247$, $b = 0.82$)	2.44	7.67	1.27	0.67
		−8%	41%	6%	−1%
(*v*)	Lump graupel fall speed ($a = 297$, $b = 0.72$)	2.84	4.33	1.13	0.65
		8%	−20%	−5%	−5%

Integrated water contents (IWCs) for each hydrometeor species (see text) are given in kg m^{-2}. Also shown is the percentage change between each case and the control case. In cases (*iii*)–(*v*), a and b represent the values of the fall-speed relationship $V = aD^b$, where V is the fall speed (m s^{-1}) and D the diameter (m), after the correction of Potter (1991) is applied.

TABLE 2. SUMMARY OF SENSITIVITY TESTS (*vi*)–(*x*)

Case	Description	IWC for q_r	IWC for q_p	IWC for q_c	IWC for q_i
(*vi*)	Enid sounding temperatures used as input	2.17	5.38	1.04	0.74
		−18%	−1%	−13%	10%
(*vii*)	Eq. (17) temperatures used as input	2.74	5.52	1.23	0.74
		4%	1%	3%	9%
(*viii*)	Eq. (17) temperatures, relative humidity = 100%	4.12	6.09	1.60	0.57
		50%*	10%*	31%*	−23%*
(*ix*)	Eq. (17) temperatures, relative humidity = 90%	3.53	5.59	1.25	0.57
		29%*	1%*	2%*	−23%*
(*x*)	Eq. (17) temperatures, relative humidity = 80%	3.00	5.52	1.26	0.69
		10%*	0%*	3%*	−7%*

Integrated water contents (IWCs) for each hydrometeor species (see text) are given in kg m^{-2}. Also shown is the percentage change between each case and the control case, except where indicated otherwise.
* % difference from case (*vii*).

TABLE 3. SUMMARY OF SENSITIVITY TESTS (*xi*)–(*xvi*)

Case	Description	IWC for q_r	IWC for q_p	IWC for q_c	IWC for q_i
(*xi*)	0131 UTC vertical-velocity profile	4.75	10.12	1.60	0.51
		80%	86%	35%	−24%
(*xii*)	0131 UTC vertical velocity, horizontal fluxes excluded ($\alpha = 0$)	4.72	10.51	1.53	0.58
		−1%*	4%*	−4%*	14%*
(*xiii*)	CP-3 radar stratiform-region vertical velocity, eddy mixing coefficient $K = 1500\ m^2 s^{-1}$	0.34	2.57	0.02	0.84
		−55%†	−32%†	−87%†	1%†
(*xiv*)	CP-4 radar stratiform-region vertical velocity, eddy mixing coefficient $K = 1500\ m^2 s^{-1}$	0.75	3.77	0.17	0.83
		−71%	−31%	−86%	23%
(*xv*)	CP-4 radar stratiform-region vertical velocity, eddy mixing coefficient $K = 2500\ m^2 s^{-1}$	1.07	4.42	0.38	0.79
		42%†	17%†	120%†	−6%†
(*xvi*)	No vertical motion ($\overline{w} = 0$), eddy mixing coefficient $K = 1500\ m^2 s^{-1}$	0.57	2.24	0.05	0.70
		−24%†	−41%†	−74%†	−16%†

Integrated water contents (IWCs) for each hydrometeor species (see text) are given in kg m^{-2}. Also shown is the percentage change between each case and the control case, except where indicated otherwise.

* % difference from case (*xi*).

† % difference from case (*xiv*).

the value of K is reduced to 1500 m^2s^{-1}, which approximately represents the minimum value of K for which the relaxation scheme will converge for the convective region vertical-velocity profile in Fig. 7. In case (*ii*), K is increased to 3500 m^2s^{-1} (Fig. 10(b)). In both cases the changes in the mixing-ratio profiles are relatively small, with changes in IWC generally less than 11%, except for the cloud-water mixing ratios, which show changes in IWC up to 18%. Therefore, the 1-D retrieval results for the convective region are not significantly dependent on the magnitude of K as long as the value is sufficiently large to allow convergence of the solution.

In cases (*iii*)–(*v*) we check the sensitivity of the retrieval results to the precipitating ice fall-speed relationship. Each fall-speed relationship was corrected according to Potter (1991). The particle types and their corresponding fall-speed relationships are listed in Table 1 and profiles of the retrieved fall speeds are shown in Fig. 11(a). The Heymsfield and Kajikawa (1987) lump graupel fall-speed relationship was used in the control case. The Locatelli and Hobbs (1974) relationships were obtained from measurements within frontal precipitation. The graupel-like snow fall-speed relationship (before the Potter correction is applied) is frequently used for modelling studies of convective systems.

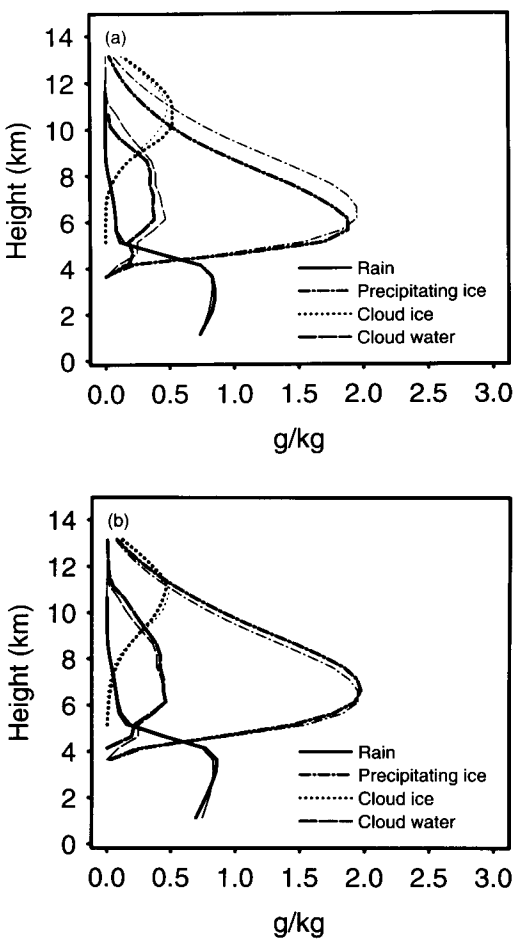

Figure 10. Same as in Fig. 9, but with the upper boundary condition for precipitating ice set to zero. The thin lines show the profiles from the control case, in which the eddy mixing coefficient $K = 2500$ m^2s^{-1}. The thick lines are for (a) $K = 1500$ m^2s^{-1} and (b) $K = 3500$ m^2s^{-1}.

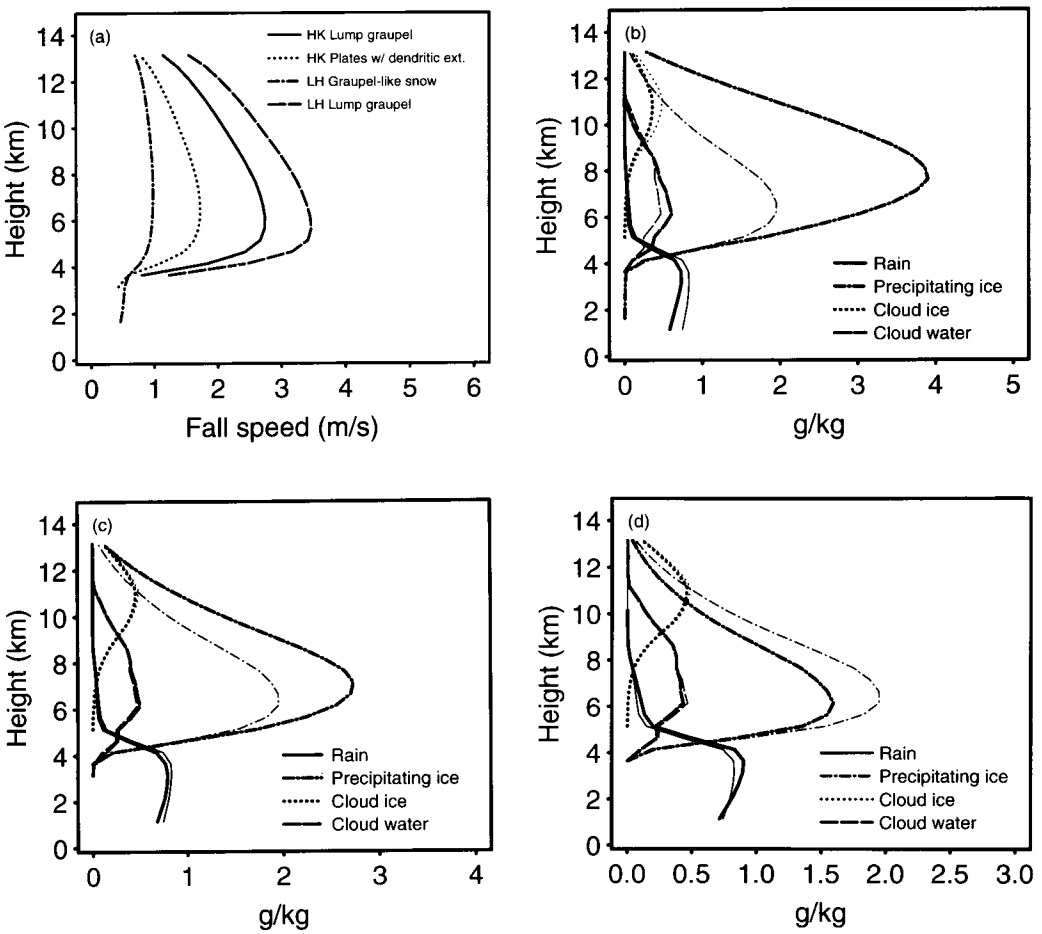

Figure 11. (a) Fall-speed profiles associated with different fall-speed relationships for precipitating ice. The fall-speed relationships are indicated in Table 1. LH and HK refer to Locatelli and Hobbs (1974) and Heymsfield and Kajikawa (1987), respectively. (b)–(d) Same as in Fig. 10, but for (b) fall-speed parameters for graupel-like snow of hexagonal type (LH), (c) fall-speed parameters for plates with dendritic extensions (HK), and (d) fall-speed parameters for lump graupel (LH). Thin lines show the profiles from the control case.

Locatelli and Hobbs (1974) provide three relationships for lump graupel (see their Table 1). We use the second relationship listed in their table since it best reproduces the graupel fall velocities observed within convective storms (Heymsfield 1978) and is frequently used to represent graupel in modelling studies.

In case (*iii*) the fall speed–diameter relationship for graupel-like snow of hexagonal type (Locatelli and Hobbs 1974) is used for precipitating ice (Fig. 11(b)). The fall speeds of the particles are significantly decreased compared with the control case and do not exceed 1 m s^{-1} (dot-dashed line in Fig. 11(a)). The reduction in fall velocities reduces the fallout rate of the precipitating-ice particles (second term on the right-hand side of (13)). As a result, precipitating-ice mixing ratios are much larger, nearly 3.9 g kg^{-1}, with a peak about 1.5 km higher than in the control case. The other profiles change only slightly. The very high values of the precipitating-ice mixing ratios and very small fall speeds in this case indicate the potential problems which may occur when snow fall speeds are applied in numerical cloud models to simulations of convective storms. In

cases of strong shear, the low fall velocities may lead to underestimates of convective rainfall and may produce excessive amounts of anvil precipitating ice.

In case (*iv*) the fall-speed relationship of Heymsfield and Kajikawa (1987) for plates with dendritic extensions, corrected according to Potter (1991), is applied to precipitating ice (Fig. 11(c)). This relationship was used by BH94 within the stratiform precipitation region in their 2-D analysis. The fall speeds for this case (dotted line in Fig. 11(a)) are greater than the graupel-like snow fall speeds, but less than those associated with graupel. As a result, the profiles for this case show peak precipitating-ice mixing-ratio values greater than in the control case, but much less than those in case (*iii*).

The lump graupel fall-speed relationship of Locatelli and Hobbs (1974) is used in case (*v*) (Fig. 11(d)). Again, the correction of Potter (1991) is applied. The fall speeds in this case (dashed line in Fig. 11(a)) are larger than those in the control run. The precipitating-ice mixing ratios are reduced by about 0.4 g kg^{-1} near 6 km compared with the control run. The smaller precipitating-ice mixing ratios result from the increased fallout rate of the precipitating-ice particles. As before, the other profiles change only slightly.

To this point, the 1-D microphysical retrieval model has been run with temperature and pressure profiles determined from the more detailed 2-D retrieval results of BH94. However, if the 1-D model is to be applied to other cases (both midlatitude and tropical), it is necessary to determine whether accurate profiles of temperature and pressure are needed, or whether crude estimates of these variables can be used. In case (*vi*) the Enid sounding, taken in the environmental air ahead of the convective line, is used to specify the temperature and pressure in the 1-D model. In case (*vii*) a temperature profile is obtained by solving an equation for the conservation of moist static energy. Following Arakawa and Schubert (1974), Johnson (1976), and Houze *et al.* (1980), an equation for the moist static energy of the updraught (h_u) is obtained by considering the conservation of h_u according to a 1-D steady-state plume model. The value of h_u as a function of height, z, and entrainment rate, λ, is given by

$$h_u(\lambda, z) = h_u(z_B)\, e^{\lambda(z_B - z)} + \lambda\, e^{-\lambda z} \int_{z_B}^{z} e^{\lambda z'} \hat{h}_u(\lambda, z')\, dz' \tag{17}$$

where $h_u(z_B)$ is the moist static energy at the base of the updraught, and $\hat{h}_u$ is the value of h entrained into the updraught, taken here as the moist static energy of the environment. If an air parcel is assumed to be saturated, then one can obtain the temperature and vapour mixing ratio of the air parcel (see Eqs. (12) and (13) of Houze *et al.* (1980)). For case (*vii*) Eq. (17) above and Eqs. (12) and (13) of Houze *et al.* (1980) are solved using an entrainment rate of 0.01 km^{-1} and using the thermodynamic data from the Enid sounding to estimate the temperature profile for the convective region. The value of $h_u(z_B)$ is determined for the lowest level using the wet-bulb potential temperature of the environment and assuming saturated conditions. For cases (*vi*) and (*vii*) the average vapour mixing ratios from the 2-D retrieval, which were used to specify the initial values for total water in the control case, are again used to specify the initial values for total water so that we can examine the sensitivity of the results to the input-temperature and pressure profiles exclusively.

Figure 12 shows profiles of the potential-temperature difference between the soundings from Enid (Fig. 3) and Eq. (17) and the mean convective region sounding from the 2-D retrieval of BH94 (Fig. 8). The Enid sounding shows potential-temperature differences of up to 6 K at low levels and −4 K at middle levels. The potential temperatures determined from (17) on the other hand show differences generally less than 2 K, which

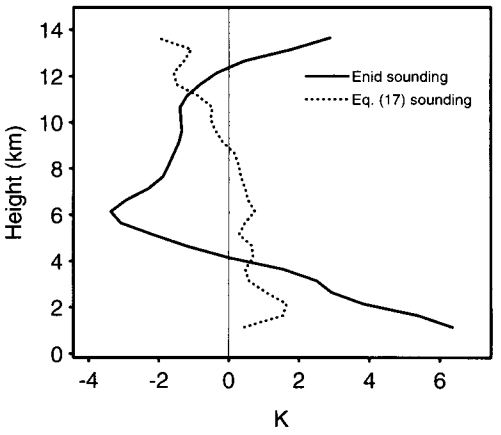

Figure 12. Potential-temperature difference between the temperature profiles obtained from the Enid 0134 UTC sounding and Eq. (17) and the convective region mean potential-temperature profile (Fig. 8) determined from the two-dimensional retrieval of Braun and Houze (1994).

suggests that (17) provides a reasonable estimate of the retrieved mean convective region temperature profile.

Mixing-ratio profiles determined from the 1-D model using the Enid temperatures as input are shown in Fig. 13(a). The melting level in the environment (4.5 km) is somewhat lower than in the convective region (4.7 km) and, as a result, the precipitating-ice mixing ratios are larger below 4.7 km. Precipitating-ice mixing ratios are also larger between the melting level and about 6 km altitude by up to 0.2 g kg^{-1}, which causes the peak in precipitating ice to occur about 0.5 km lower. The total rain-water content is 18% lower than in the control case. The shape of the vertical profile of cloud-water mixing ratio has been modified, although the total water content associated with cloud water has changed by only 13% (Table 2).

Improvements can be made by using the in-cloud sounding estimated from the environmental sounding. The hydrometeor profiles determined for this case are shown in Fig. 13(b). The retrieved hydrometeor profiles are nearly identical to those in the

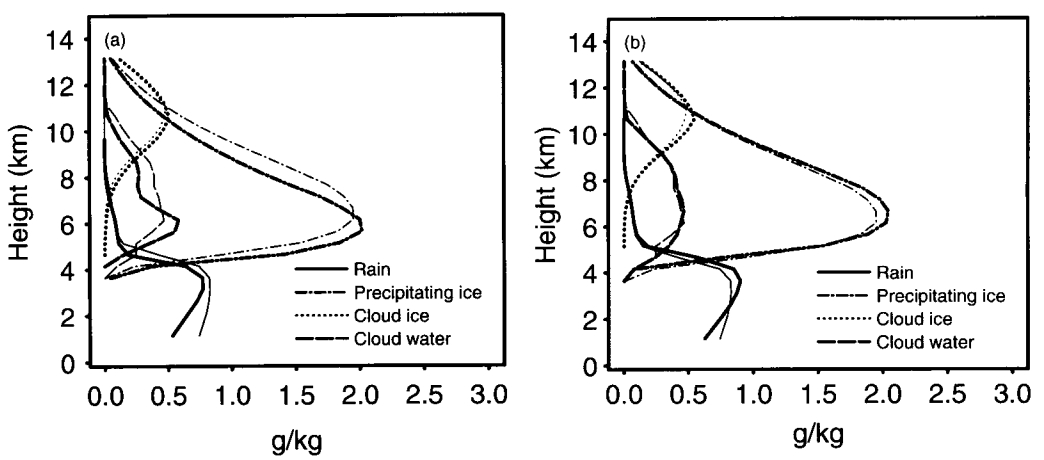

Figure 13. Same as in Fig. 10, but for a temperature profile determined from (a) the Enid sounding at 0134 UTC 11 June 1985 and (b) from Eq. (17). Thin lines show the profiles from the control case.

control case since the temperatures approximated from (17) are similar to the mean in-cloud temperatures determined from the 2-D retrieval of BH94.

Since in-cloud thermodynamic data will generally not be available, (17) can be used to estimate the mean in-cloud temperatures. However, vapour mixing ratios, which are used to specify the initial values of the total-water mixing ratio, will also be unavailable and must be estimated from the temperature profile, i.e. from the saturation vapour mixing ratio. Therefore, three tests are conducted to determine the sensitivity of the results to the input water-vapour profile. For cases (*viii*)–(*x*) the mean temperatures are estimated from (17) and the initial vapour mixing ratios are estimated by assuming relative humidities of 100, 90, and 80 per cent, respectively. Figure 14 shows the hydrometeor profiles for each case compared with those from case (*vii*) (indicated by the thin lines in Fig. 14). As can be seen in the figure and from the data in Table 2, the most substantial sensitivity appears to occur in the rain profile and in the cloud-water profile below about 5 km. The largest differences from case (*vii*) are associated with an initial relative humidity of 100%, while for 80% relative humidity the differences are small. The large differences at low levels in cases (*viii*) and (*ix*) Figs. 14(a) and (b) are due to the overestimate of the relative humidity below 5 km. In the mean vapour mixing-

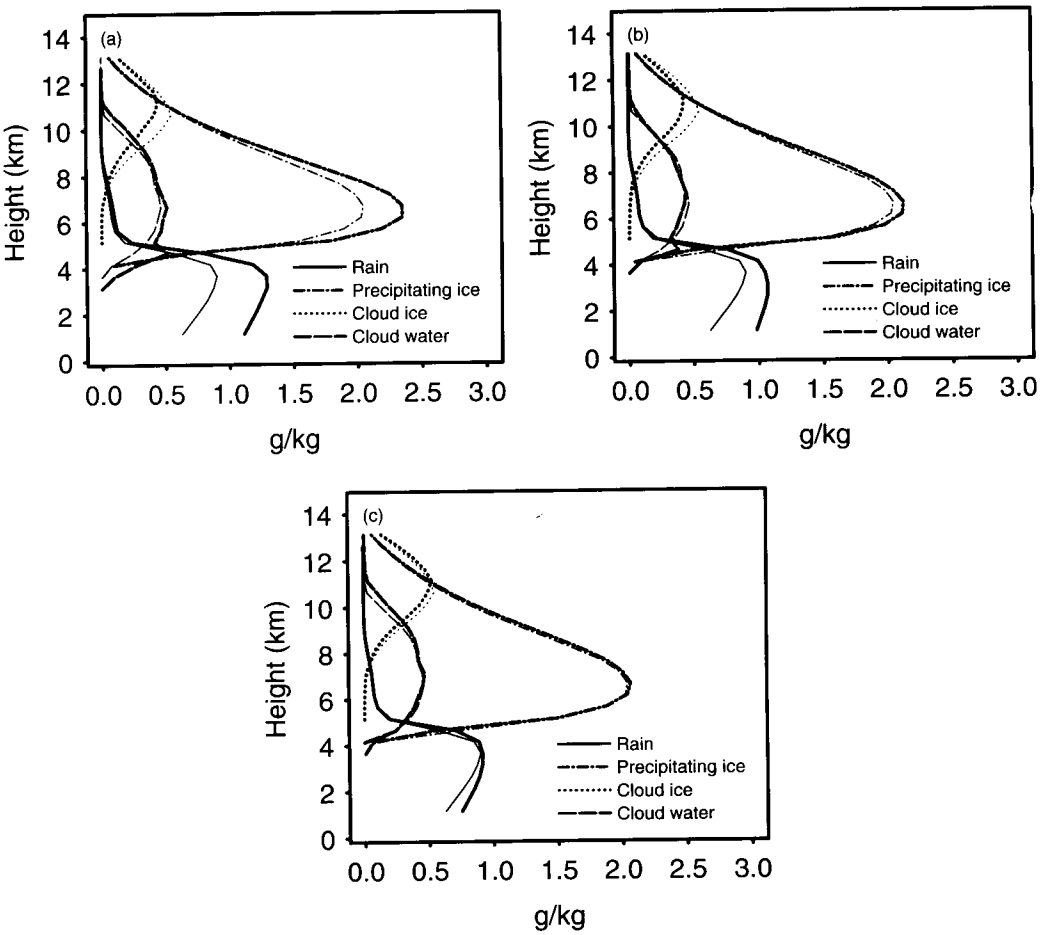

Figure 14. Same as Fig. 13(b), but for total water mixing ratios initialized from saturated vapour mixing ratios and relative humidities of (a) 100%, (b) 90%, and (c) 80%. Thin lines indicate the profiles for case (*vii*).

ratio profile determined from the 2-D results of BH94, the relative humidity increases from 77 to 95% between 1 and 4 km because of the effects of convective downdraughts. The sensitivity of the 1-D retrieval to the relative humidity at lowest levels is apparently related to the importance of the horizontal flux of water vapour in the convective region (Fig. 1(c)).

As mentioned in BH94, the vertical velocities in the composite radar data set tend to be less than those of the individual dual-Doppler volumes as a result of averaging and filtering. A mean vertical-velocity profile (Fig. 15) determined from the 0131 UTC dual-Doppler volume by averaging over the box indicated in Fig. 1(a) shows maximum ascent at the same height as the composite data (Fig. 7), but with a magnitude approximately twice as large. The much stronger mean vertical velocities made it necessary to increase the value of K to 3000 m^2s^{-1} in order to obtain a convergent solution. When the 0131 UTC vertical-velocity profile is used in the retrieval (case (*xi*)) the precipitating-ice mixing ratios (Fig. 16(a)) are substantially increased to about 3.6 g kg^{-1}, while the rain mixing ratios reach up to 1.5 g kg^{-1}. Thus, the model is quite sensitive to the magnitude of the mean ascent, as should be the case for this method to be useful. The accuracy of the mixing-ratio profiles, therefore, will depend on the accuracy of the vertical-velocity profile.

In section 2 the horizontal fluxes were estimated from the 0131 UTC dual-Doppler radar data and were shown to be small compared with the vertical fluxes for rain, precipitating ice, and cloud ice. In case (*xii*) we confirm that the effects of the horizontal fluxes are small by setting the value of α in the equations for rain, precipitating ice, and cloud ice to zero, thereby removing the mean component of the horizontal flux from (13). Figure 16(b) shows the mixing-ratio profiles for case (*xii*) (thick lines) overlaid on the profiles for case (*xi*) (thin lines), which included the horizontal fluxes. It can be seen that exclusion of the horizontal fluxes produces only small changes in the vertical profiles of rain and precipitating ice. Larger changes occur in the cloud-ice profile, with the cloud-ice IWC reduced by about 14%.

To demonstrate further the sensitivity of the model to the vertical-velocity profile, we apply the model to mean vertical motions typical of the stratiform precipitation regions of squall lines. We use average vertical-velocity data obtained from the CP-3 and CP-4 radars on 11 June 1985 by Rutledge *et al.* (1988a) using the EVAD method (Srivastava *et al.* 1986). The CP-3 and CP-4 vertical-velocity profiles (Fig. 17) are

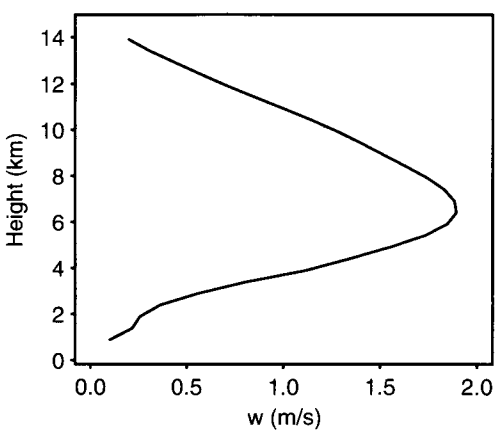

Figure 15. Mean vertical velocity (m s^{-1}) in the convective region for 0131 UTC 11 June 1985 determined from the box in Fig. 1(a).

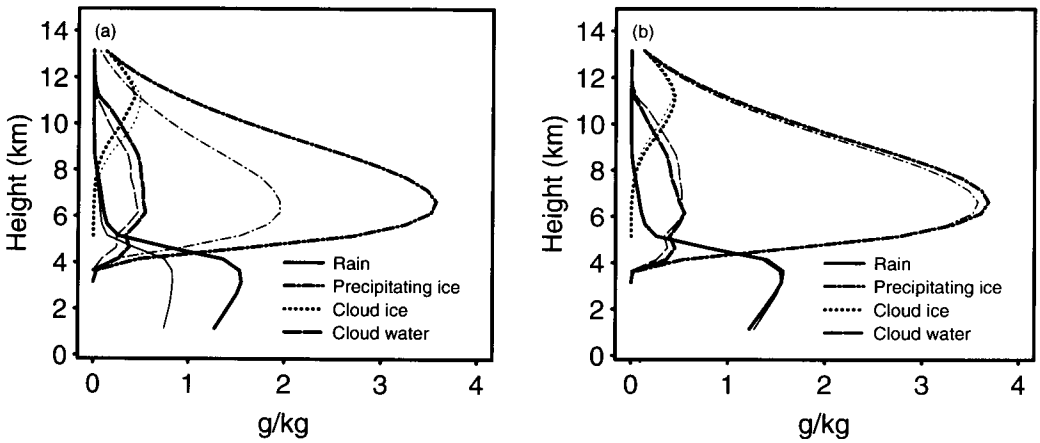

Figure 16. (a) As in Fig. 10, but for the 0131 UTC 11 June 1985 vertical-velocity profile. Thin lines show the profiles from the control case. (b) As in (a), but with the horizontal flux terms for rain, precipitating ice, and cloud ice removed by setting $\alpha = 0$. Thin lines indicate the 0131 UTC profiles from (a).

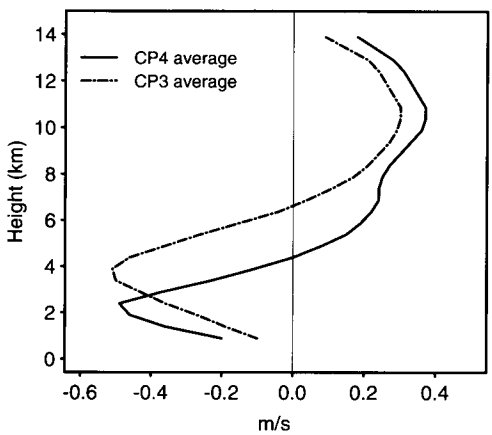

Figure 17. Mean vertical velocities (m s^{-1}) in the stratiform region of the 11 June 1985 squall line determined from the EVAD analysis of Rutledge *et al.* (1988a, see their Fig. 15). The profiles are determined from time averages for the CP-3 and CP-4 radars.

typical of stratiform-region vertical motions (Houze 1989). The CP-4 profile, which is characteristic of the enhanced reflectivity zone in the secondary band, shows ascent (0.2 to 0.4 m s^{-1}) above 4 km and descent (~0.5 m s^{-1}) below this level. The CP-3 profile is more characteristic of the rear portion of the stratiform region, with weaker ascent and somewhat deeper descent.

For the stratiform-region retrievals the mixing coefficient was reduced to 1500 $m^2 s^{-1}$ since we expect the vertical mixing to be less than in the convective region. The fall-speed relationship of Heymsfield and Kajikawa (1987) for plates with dendritic extensions was used for precipitating ice since graupel was not present in substantial amounts in the stratiform region of the 10–11 June squall line (Rutledge *et al.* 1988b). As discussed in section 2, the values of α for rain, precipitating ice, and cloud ice are set to unity for the stratiform region. The average temperature and pressure profiles used previously for the convective region are used in the following cases to simplify the comparison with the

prior test cases. Braun and Houze (1995) show hydrometeor profiles that occur when a stratiform-region sounding is used to specify the thermodynamic profiles.

Figure 18(a) shows the retrieved hydrometeor profiles diagnosed from the CP-3 and CP-4 mean vertical-velocity profiles (cases (*xiii*) and (*xiv*) respectively). The rain and precipitating-ice mixing ratios are substantially less than the convective-region values (Table 3, Figs. 9 and 16). For the CP-4 profiles the precipitating-ice mixing ratios peak near 7 km at approximately 1.3 g kg^{-1}, while the rain mixing ratios are about 0.25 g kg^{-1}. Small amounts of cloud water are found within the mesoscale updraught between 6 and 9 km altitude. The weaker ascent and deeper descent in the CP-3 vertical-motion profile leads to less precipitating ice aloft and approximately half as much rain at low levels.

Caution must be exercised when applying the 1-D retrieval model to stratiform precipitation regions with weak mean vertical motion. Figure 18(b) shows the mixing-ratio profiles for the CP-4 mean vertical-motion profile for K equal to 1500 m^2s^{-1} (thin lines, case (*xiv*)) and K equal to 2500 m^2s^{-1} (thick lines, case (*xv*)). In contrast to the

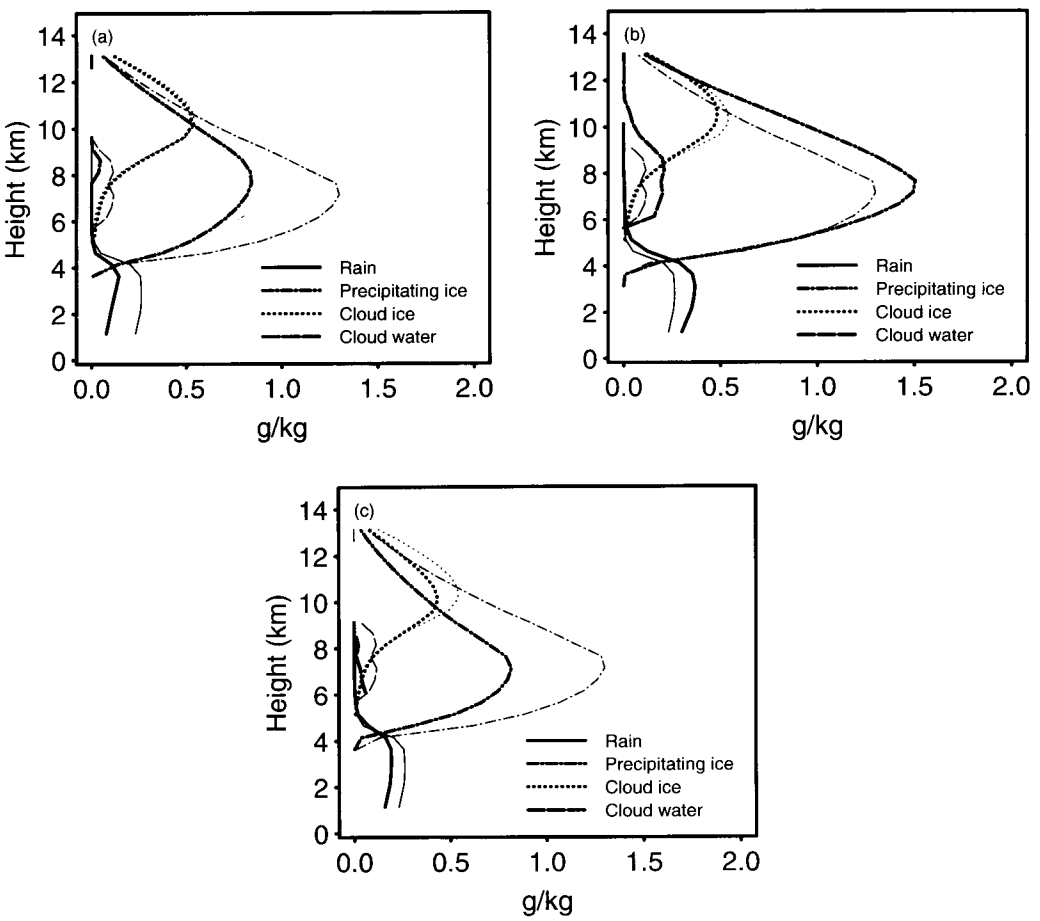

Figure 18. (a) Hydrometeor profiles determined from the stratiform-region vertical-motion profiles in Fig. 17. The thin (thick) lines indicate profiles for the CP-4 (CP-3) radar vertical-motion profile. (b) Hydrometeor profiles for the CP-4 radar vertical motions. The thin lines indicate the profiles for the eddy mixing coefficient $K = 1500\ m^2s^{-1}$ (from Fig. 18(a), thin lines), while the thick lines indicate profiles for $K = 2500\ m^2s^{-1}$. (c) Hydrometeor profiles for the no vertical motion case (thick lines). The thin lines indicate the CP-4 radar profiles from Fig. 18(a).

results for the convective region, the profiles for the stratiform region show greater sensitivity to the value of K (Table 3). Additional tests (not shown) indicate that the retrieved mixing-ratio values are increasingly sensitive to the mixing term as the magnitude of the vertical motion decreases.

In the extreme case in which $\overline{w} = 0$ (case (*xvi*), thick lines in Fig. 18(c)), significant precipitation amounts are still deduced by the retrieval model, with the magnitudes of the mixing ratios determined by the strength of the vertical mixing ($K = 1500\ \mathrm{m^2 s^{-1}}$ in this case). This case represents an extreme end in the spectrum of stratiform clouds in which the microphysics within the cloud are controlled not by the mean vertical motions but by the turbulent mixing within the cloud, reminiscent of the processes that are active in fog. The differences in the profiles between case (*xvi*) and case (*xiv*) (indicated by the thin lines in Fig. 18(c)) are indicative of the effects of the vertical motion. Above the melting level, ascent enhances the ice mixing ratios. Only a small difference is seen below the melting level, but this result occurs because the enhancement of precipitation by the ascent above the melting level is virtually negated by the enhanced evaporation within the mesoscale descent.

Of course, such a large mixing coefficient is probably unrealistic when the vertical motion is zero. A smaller mixing coefficient reduces the mixing ratios. Although the model did not converge for values of K less than $850\ \mathrm{m^2 s^{-1}}$, one can infer that the mixing ratios will decrease toward zero as K goes to zero. Because of the greater sensitivity of the results to K when the vertical motions are weak, and the difficulty of obtaining solutions for very low values of K, there is greater uncertainty in the retrieved mixing ratios within the stratiform region, particularly when the vertical motions are less than about $20\ \mathrm{cm\ s^{-1}}$.

5. Potential applications

(*a*) *Microwave measurements*

The purpose of the TRMM is to measure the global distribution of precipitation using spaceborne radars and microwave radiometers. As discussed by Simpson *et al.* (1988), an understanding of the relationships between cloud radiative and microphysical–dynamical processes is crucial to the successful retrieval of precipitation rates from spaceborne or high-altitude airborne microwave measurements. The 1-D microphysical retrieval model developed in this paper may provide a means for improving such satellite retrieval techniques, or for obtaining more detailed information for ground-truth studies. The vertical distributions of the hydrometeor species, which can be determined from the microphysical retrieval model described here, strongly influence the microwave radiances. The output from the 1-D retrieval can be used in conjunction with a radiative-transfer model to retrieve precipitation amounts and vertical structure from brightness temperatures for different frequencies. The better description of the vertical distribution of hydrometeors and the more refined partitioning of the total water content between liquid and ice as well as between cloud and precipitation provided by the 1-D retrieval model may potentially be used to:

- Extend ground-truth data by providing information on the mean vertical distribution of the hydrometeor fields other than those that can be determined by radar observations.
- Improve retrievals of the vertical structure of precipitating systems from satellite (Kummerow *et al.* 1991; Kummerow and Giglio 1994) by providing more relevant validation information on hydrometeor profiles.

- Provide a constraint for the mean liquid water contents retrieved from satellite microwave measurements.
- Indicate vertical cloud and precipitation structures for different types of cloud systems in different environments.

(*b*) *Diabatic-heating profiles*

The 1-D retrieval model may also allow for determining heating rates from the vertical hydrometeor profiles (Tao *et al.* 1990, 1993). Vertical hydrometeor profiles retrieved from satellite measurements are fairly crude at this time because of the approximate nature by which these vertical structures are defined in the retrieval algorithms. Consequently, the hydrometeor profiles retrieved from satellites will probably have insufficient vertical resolution and inadequate discrimination of the hydrometeor species for estimating heating rates from the hydrometeor/heating algorithms of Tao *et al.* (1990, 1993). If the 1-D retrieval model is used to define better the vertical structures of precipitating systems such that retrievals from satellites are significantly improved, then the hydrometeor/heating algorithms of Tao *et al.* (1990, 1993) will become more powerful.

Braun and Houze (1995) describe the distribution of melting and freezing rates in the convective and stratiform precipitation areas of the 10–11 June 1985 squall line. Using the retrieval results of BH94 they show that the cooling by melting in the convective region is quite intense and contributes nearly an equal amount as the stratiform region to the total cooling by melting in the squall line, despite the smaller areal coverage of the convective line compared with the stratiform region. The implication is that cooling by melting in the convective region is a significant component of the heat budget of the 0–11 June squall line and probably other midlatitude convective systems. While methods are available for estimating melting rates from radar-reflectivity profiles within stratiform precipitation (e.g. Leary and Houze 1979), no methods have been available for estimating melting and freezing rates within convection. The microphysical parametrizations of the 1-D microphysical retrieval model now offer a means to determine these heating and cooling rates. This subject is discussed in detail in Braun and Houze (1995).

(*c*) *Wide applicability*

From multiple-Doppler data one can perform microphysical retrievals in one, two, or even three dimensions. However, multiple-Doppler data are often unavailable. A key advantage of the 1-D retrieval technique is that it can be applied to single-Doppler data. A vertical profile of area-mean divergence obtained by a single Doppler radar can be integrated vertically to yield an area-mean vertical-velocity profile, which can then be used as input for the 1-D retrieval model. Methods such as VAD and EVAD are not required to obtain the divergence profiles. VAD and EVAD assume a linearly varying wind field to obtain the mean winds and shearing and stretching deformations. This linearity assumption is *not* required to obtain the divergence. Thus, information on the vertical distribution of the microphysical variables can be obtained at sites equipped with single-Doppler radars (e.g. TRMM ground-truth sites). When Doppler data are unavailable, an alternative approach is to estimate the cloud mass fluxes from radar-derived rainfall and cloud-top height measurements as described by Austin and Houze (1973) and Houze *et al.* (1980). The in-cloud temperatures can then be approximated from Eq. (17) given a sounding in the near-storm environment. Thus, crude estimates of the vertical profiles of hydrometeors can be obtained even when the radar reflectivity from a single radar is all that is available.

6. Conclusions

A simple one-dimensional microphysical retrieval model has been developed for estimating vertical profiles of liquid and frozen hydrometeors from an input vertical profile of vertical velocity. Sensitivity tests indicate that the retrieval model is somewhat sensitive to the choice of fall-speed parameters for precipitating ice (snow versus graupel, Fig. 11) and to the initial guess of the total water content at lowest levels (Fig. 14). For regions of convection the model is fairly insensitive to the value of the mixing coefficient (Fig. 10) and to small changes in the input-temperature profile (Fig. 13). The relative lack of sensitivity to the input-temperature profile enables one to approximate the in-cloud temperature profile from a single sounding in the storm's environment. Based upon the assumptions made in the derivation of the equations for the retrieval model in section 2, and the results of the sensitivity tests in section 4, we expect that the model will have the following limitations when applied to regions of convection:

- The accuracy of the mixing-ratio profiles depends primarily on the accuracy of the mean vertical-velocity profile. This sensitivity to the vertical velocity is necessary if the retrieval technique is to be useful.
- The accuracy of the rain mixing ratios depends on the initial values of total water at low levels (Fig. 14).
- The accuracy of the precipitating-ice mixing ratios depends on the assumed form of the precipitating ice, e.g. snow or graupel (Fig. 11).
- Accurate profiles can only be retrieved if the horizontal eddy flux term in (7) is negligible and if the perimeter mean value of the mixing ratios can be related to the in-cloud values through a simple function as in (12).
- The error in the microphysical source terms will increase with increasing in-cloud temperature variability near the melting level (section 2, Fig. 5).

In stratiform precipitation regions the results show some sensitivity to the value of the mixing coefficient (Fig. 18(a)). The sensitivity of the results to the mixing coefficient increases as the magnitude of the vertical motion decreases. Therefore, the 1-D retrieval model may not work as effectively when the vertical motion becomes $\leq 20\ \mathrm{cm\ s^{-1}}$. In such weak vertical-motion cases, kinematic models such as that used by Zrnic *et al.* (1993) may provide better results.

The retrieval model may be useful for improving or validating precipitation measurements from spaceborne radar and microwave radiometer measurements such as those to be obtained by the TRMM satellite (Simpson *et al.* 1988). It can also be used for estimating heating rates, including melting and freezing rates for the convective and stratiform regions of squall lines as described in Braun and Houze (1995). While the 1-D retrieval model is limited to retrieval of only the area-mean profiles of the mixing-ratio fields (compared with 2-D or 3-D calculations), it has the following advantages:

- The calculations can be performed quickly.
- Input requirements are less restrictive. The 1-D model requires an area-mean vertical-velocity profile, which can be obtained by either dual- or single-Doppler velocity information (EVAD is not required, see section 5(c)). Thermodynamic inputs (temperature and pressure) can generally be approximated from an environmental sounding and a simple steady-state plume model governing the conservation of moist static energy (17).
- The stationarity assumption for the area mean is less restrictive than steady-state calculations for retrievals in two or three dimensions since the stationarity of the mean does not require the internal structure of the storm to be in steady state at all points.

- The hydrometeor profiles are closely linked to velocity measurements taken within the storm rather than to cloud model-derived fields (as described by Simpson *et al.* (1988)) whose only link to a given storm is the environmental sounding used to initiate the model storm.

ACKNOWLEDGEMENTS

We would like to thank Professor M. Biggerstaff for supplying us with the synthesized dual-Doppler radar data set used in this study and Professors R. G. Fovell and Y. Ogura for providing the cloud model fields used to test the microphysical retrieval program. We also thank Dr W.-K. Tao, Sandra Yuter, Ming-Jen Yang, and the two reviewers of this manuscript for their helpful comments. G. C. Gudmundson edited the manuscript. This research was sponsored by National Science Foundation grant ATM-9101653 and National Aeronautics and Space Administration grant NAG 5 1599.

REFERENCES

Arakawa, A. and Schubert, W. 1974 Interaction of a cumulus cloud ensemble with the large-scale environment. Part I. *J. Atmos. Sci.*, **35**, 674–701

Austin, P. M. and Houze Jr, R. A. 1973 A technique for computing vertical transports by precipitating cumuli. *J. Atmos. Sci.*, **30**, 1100–1111

Biggerstaff, M. I. and Houze Jr, R. A. 1991a Kinematic and precipitation structure of the 10–11 June 1985 squall line. *Mon. Weather Rev.*, **119**, 3034–3065

1991b Midlevel vorticity structure of the 10–11 June 1985 squall line. *Mon. Weather Rev.*, **119**, 3066–3079

1993 Kinematics and microphysics of the transition zone of the 10–11 June 1985 squall line. *J. Atmos. Sci.*, **50**, 3091–3110

Braun, S. A. and Houze Jr, R. A. 1994 The transition zone and secondary maximum of radar reflectivity behind a midlatitude squall line: Results retrieved from Doppler radar data. *J. Atmos. Sci.*, **51**, 2733–2755

1995 Melting and freezing in a mesoscale convective system. *Q. J. R. Meteorol. Soc.*, **121**, 55–77

Chong, M. and Hauser, D. 1989 A tropical squall line observed during the COPT 81 experiment in West Africa. Part II: Water budget. *Mon. Weather Rev.*, **117**, 728–744

1990 A tropical squall line observed during the COPT 81 experiment in West Africa. Part III: Heat and moisture budgets. *Mon. Weather Rev.*, **118**, 1696–1706

Churchill, D. D. and Houze Jr, R. A. 1984 Mesoscale updraft magnitude and cloud-ice content deduced from the ice budget of the stratiform region of a tropical cloud cluster. *J. Atmos. Sci.*, **41**, 1717–1725

Cunning, J. B. 1986 The Oklahoma–Kansas preliminary regional experiment for STORM-Central. *Bull. Am. Meteorol. Soc.*, **67**, 1478–1486

Ferrier, B. S. and Houze Jr, R. A. 1989 One-dimensional time-dependent modeling of GATE cumulonimbus convection. *J. Atmos. Sci.*, **46**, 330–352

Fovell, R. G. and Ogura, Y. 1988 Numerical simulation of a midlatitude squall line in two dimensions. *J. Atmos. Sci.*, **45**, 3846–3879

Fritsch, J. M., Kane, R. J. and Chelius, C. R. 1986 The contribution of mesoscale convective weather systems to the warm-season precipitation in the U.S. *J. Clim. Appl. Meteorol.*, **25**, 1333–1345

Fulton, R. and Heymsfield, G. M. 1991 Microphysical and radiative characteristics of convective clouds during COHMEX. *J. Appl. Meteorol.*, **30**, 98–116

Gal-Chen, T. 1982 Errors in fixed and moving frame of references: Applications for conventional and Doppler radar analysis. *J. Atmos. Sci.*, **39**, 2279–2300

Gunn, K. L. S. and Marshall, J. S. 1958 The distribution with size of aggregate snowflakes. *J. Meteorol.*, **15**, 452–461

Hakkarinen, I. M. and Adler, R. F. 1988 Observations of precipitating convective systems at 92 and 183 GHz: Aircraft results. *Meteorol. Atmos. Phys.*, **38**, 164–182

Hauser, D., Roux, F. and Amayenc, P. 1988 Comparison of two methods for the retrieval of thermodynamic and microphysical variables from Doppler-radar measurements: Application to the case of a tropical squall line. *J. Atmos. Sci.*, **45,** 1285–1303

Heymsfield, A. J. 1978 The characteristics of graupel particles in northeastern Colorado cumulus congestus clouds. *J. Atmos. Sci.*, **35,** 284–295

Heymsfield, A. and Hjelmfelt, M. R. 1984 Processes of hydrometeor development in Oklahoma convective clouds. *J. Atmos. Sci.*, **41,** 2811–2835

Heymsfield, A. and Kajikawa, M. 1987 An improved approach to calculating terminal velocities of plate-like crystals and graupel. *J. Atmos. Sci.*, **44,** 1088–1099

Houze Jr, R. A. 1973 A climatological study of vertical transports by cumulus-scale convection. *J. Atmos. Sci.*, **30,** 1112–1123

1989 Observed structure of mesoscale convective systems and implications for large-scale heating. *Q. J. R. Meteorol. Soc.*, **115,** 424–461

Houze Jr, R. A., Cheng, C.-P., Leary, C. A. and Gamache, J. F. 1980 Diagnosis of cloud mass and heat fluxes from radar and synoptic data. *J. Atmos. Sci.*, **37,** 754–772

Johnson, R. H. 1976 The role of convective-scale downdrafts in cumulus and synoptic-scale interactions. *J. Atmos. Sci.*, **33,** 1890–1910

1984 Partitioning tropical heat and moisture budgets into cumulus and mesoscale components: Implications for cumulus parameterization. *Mon. Weather Rev.*, **112,** 1590–1601

Johnson, R. H. and Hamilton, P. J. 1988 The relationship of surface pressure features to the precipitation and airflow structure of an intense midlatitude squall line. *Mon. Weather Rev.*, **116,** 1444–1472

Kessler, E. 1969 On the distribution and continuity of water substance in atmospheric circulations. Meteorol. Monograph., No. 32. Am. Meteorol. Soc.

Kummerow, C. and Giglio, L. 1994 A passive microwave technique for estimating rainfall and vertical structure information from space. Part I: Algorithm description. *J. Appl. Meteorol.*, **33,** 3–18

Kummerow, C., Hakkarinen, I. M., Pierce, H. F. and Weinmann, J. A. 1991 Determination of precipitation profiles from airborne passive microwave radiometric measurements. *J. Atmos. Ocean. Technol.*, **8,** 148–158

Leary, C. A. and Houze Jr, R. A. 1979 Melting and evaporation of hydrometeors in precipitation from anvil clouds of deep tropical convection. *J. Atmos. Sci.*, **36,** 669–679

1980 The contribution of mesoscale motions to the mass and heat fluxes of an intense tropical convective system. *J. Atmos. Sci.*, **37,** 784–796

Lin, Y.-L., Farley, R. D. and Orville, H. D. 1983 Bulk parameterization of the snow field in a cloud model. *J. Clim. Appl. Meteorol.*, **22,** 1065–1092

Locatelli, J. D. and Hobbs, P. V. 1974 Fall speed and masses of solid precipitation particles. *J. Geophys. Res.*, **79,** 2185–2197

Marécal, V., Hauser, D. and Roux, F. 1993 The 12–13 January 1988 narrow cold-frontal rainband observed during MFDP/FRONTS 87. Part II: Microphysics. *J. Atmos. Sci.*, **50,** 975–998

Olsen, W. S. 1989 Physical retrieval of rainfall rates over the ocean by multispectral microwave radiometry: Application to tropical cyclones. *J. Geophys. Res.*, **94,** 2267–2280

Palmén, E. and Newton, C. W. 1969 *Atmospheric circulation systems: Their structure and physical interpretation.* Academic Press, New York

Potter, B. E. 1991 Improvements to a commonly used cloud microphysical bulk parameterization. *J. Clim. Appl. Meteorol.*, **30,** 1040–1042

Riehl, H. and Malkus, J. S. 1958 On the heat balance in the equatorial trough zone. *Geophysica*, **6,** 503–538

Rogers, R. R. and Yau, M. K. 1989 *A short course in cloud physics.* Third Edition. Pergamon Press

Roux, F., Testud, J., Payen, M. and Pinty, B. 1984 West African squall-line thermodynamic structure retrieved from dual-Doppler radar observations. *J. Atmos. Sci.*, **41,** 3104–3121

Rutledge, S. A. and Hobbs, P. V. 1983 The mesoscale and microscale structure and organization of clouds and precipitation in midlatitude cyclones. VIII: A model for the "seeder–feeder" process in warm frontal rainbands. *J. Atmos. Sci.*, **40,** 1185–1206

1984 The mesoscale and microscale structure and organization of clouds and precipitation in midlatitude cyclones. XII: A diagnostic modeling study of precipitation development in narrow cold-frontal rainbands. *J. Atmos. Sci.*, **41,** 2949–2972

Rutledge, S. A. and Houze Jr, R. A. 1987 A diagnostic modeling study of the trailing stratiform region of a midlatitude squall line. *J. Atmos. Sci.*, **44,** 2640–2656

Rutledge, S. A., Houze Jr, R. A., Biggerstaff, M. I. and Matejka, T. 1988a The Oklahoma–Kansas mesoscale convective system of 10–11 June 1985: Precipitation structure and single-Doppler radar analysis. *Mon. Weather Rev.*, **116,** 1409–1430

Rutledge, S. A., Houze Jr, R. A., Heymsfield, A. J. and Biggerstaff, M. I. 1988b 'Dual-Doppler and airborne microphysical observations in the stratiform region of the 10–11 June MCS over Kansas during PRE-STORM'. Pp. 705–707 in Preprints of the Tenth International Cloud Physics Conference, Offenbach am Main. Deutscher Wetterdienst

Simpson, J., Adler, R. F. and North, G. R. 1988 A proposed Tropical Rainfall Measuring Mission (TRMM) satellite. *Bull. Am. Meteorol. Soc.*, **69,** 278–295

Smith, E. A., Mugnai, A., Cooper, H. S., Tripoli, G. J. and Xiang, X. 1992 Foundations for statistical–physical precipitation retrieval from passive microwave satellite measurements. Part 1: Brightness-temperature properties of a time-dependent cloud-radiation model. *J. Appl. Meteorol.*, **31,** 506–531

Srivastava, R. C., Matejka, T. J. and Lorello, T. J. 1986 Doppler-radar study of the trailing-anvil region associated with a squall line. *J. Atmos. Sci.*, **43,** 356–377

Sun, J. and Houze Jr, R. A. 1992 Validation of a thermodynamic retrieval technique by application to a simulated squall line with trailing stratiform precipitation. *Mon. Weather Rev.*, **120,** 1003–1018

Sun, J., Braun, S. A., Biggerstaff, M. I., Fovell, R. G. and Houze Jr, R. A. 1993 Warm upper-level downdrafts associated with a squall line. *Mon. Weather Rev.*, **121,** 2919–2927

Tao, W.-K., Simpson, J., Lang, S., McCumber, M., Adler, R. and Penc, R. 1990 An algorithm to estimate the heating budget from vertical hydrometeor profiles. *J. Appl. Meteorol.*, **29,** 1232–1244

Tao, W.-K., Lang, S., Simpson, J. and Adler, R. 1993 Retrieval algorithms for estimating the vertical profiles of latent heat release: Their applications for TRMM. *J. Meteorol. Soc. Japan*, **71,** 685–700

Tetens, O. 1930 Uber einige meteorologische begriffe. *Z. Geophys.*, **6,** 297–309

Thiele, O. W. (Ed.) 1987 'On requirements for a satellite mission to measure tropical rainfall'. NASA Ref. Pub. 1183

Wilheit, T. T., King, J. L., Rodgers, E. B., Nieman, R. A., Krupp, B. M., Milman, A. S., Stratigos, J. S. and Siddalingaiah, H. 1982 Microwave radiometric observations near 19, 35, 37, 92, and 183 GHz of precipitation in tropical storm Cora. *J. Appl. Meteorol.*, **21,** 1137–1145

Yanai, M., Esbensen, S. and Chu, J. H. 1973 Determination of bulk properties of tropical cloud clusters from large-scale heat and moisture budgets. *J. Atmos. Sci.*, **30,** 611–627

Ziegler, C. L. 1985 Retrieval of thermal and microphysical variables in observed convective storms. Part 1: Model development and preliminary testing. *J. Atmos. Sci.*, **42,** 1487–1509

Zrnic, D. S., Balakrishnan, N., Ziegler, C. L., Bringi, V. N., Aydin, K. and Matejka, T. 1993 Polarimetric signatures in the stratiform region of a mesoscale convective system. *J. Appl. Meteorol.*, **32,** 678–693